



Impact of building density on natural ventilation potential and cooling energy saving across Chinese climate zones

Xiaoxiong Xie^a, Zhiwen Luo^{b,*}, Sue Grimmond^c, Ting Sun^d

^a School of the Built Environment, University of Reading, United Kingdom

^b Welsh School of Architecture, Cardiff University, United Kingdom

^c Department of Meteorology, University of Reading, United Kingdom

^d Institute for Risk and Disaster Reduction, University College London, United Kingdom

ARTICLE INFO

Keywords:

Natural ventilation
Urban climate
Land surface model
EnergyPlus
Climate zone

ABSTRACT

Natural ventilation is an energy-efficient approach to reduce the need for mechanical ventilation and air conditioning in buildings. However, traditionally weather data for building energy simulation are obtained from rural areas, which do not reflect the urban micrometeorological conditions. This study combines the Surface Urban Energy and Water Balance Scheme (SUEWS) and EnergyPlus to predict natural ventilation potential (NVP) and cooling energy saving in three idealised urban neighbourhoods with different urban densities in five Chinese cities of different climate zones. SUEWS downscales the meteorological inputs required by EnergyPlus, including air temperature, relative humidity, and wind speed profiles. The findings indicate that NVP and cooling energy saving differences between urban and rural areas are climate- and season-dependent. During summer, the urban-rural differences in natural ventilation hours are -43% to 10% (cf. rural) across all climates, while in spring/autumn, they range from -7% to 36% . The study also suggests that single-sided ventilation can be as effective as cross ventilation for buildings in dense urban areas. Our findings highlight the importance of considering local or neighbourhood-scale climate when evaluating NVP. We demonstrate a method to enhance NVP prediction accuracy in urban regions using EnergyPlus, which can contribute to achieving low-carbon building design.

1. Introduction

The Paris Agreement calls on countries to cut carbon emissions to meet the target of limiting global warming to preferably $1.5\text{ }^{\circ}\text{C}$ compared to pre-industrial levels [1]. In 2019, carbon emissions from the operation of buildings accounted for 28% of total global energy-related carbon emissions [2]. Although in China building operation contributes to 21.6% of national carbon emissions [3], China's building energy consumption is expected to continue to rise with urbanisation and climate change. Thus, it is important but challenging to improve energy efficiency.

Natural ventilation is a key passive cooling strategy used to achieve low-carbon building design. It reduces energy consumption, and improves occupants' health, comfort, and productivity [4]. As the effectiveness of natural ventilation depends on the outdoor weather conditions, these impacts need to be assessed.

Natural ventilation potential (NVP) is defined as the possibility (or probability) of achieving acceptable indoor thermal comfort and air

quality through natural ventilation alone [5]. Although studies worldwide using different methods and metrics (Table 1), assessing NVP can be difficult due to its sensitivity to factors such as weather, climate, building design, and the surrounding environment [12]. Current methods can be generally categorised into climate-based and building simulation based approaches [27].

Climate-based approaches provide broad geographic NVP variations using outdoor air temperature and wind speed [27], for use in the early design stage when detailed building information is unavailable (outdoor data analysis, Table 1). For example, Chen et al.'s (2017) global analysis using typical meteorological year (TMY) data found temperate climates (e.g. subtropical highland, Mediterranean) tend to have larger NVP compared to more extreme climates (e.g. tropical, subarctic). Humidity is also identified as being important when assessing NVP in hot-humid climates [19].

Using building energy simulation tools (e.g. EnergyPlus [31,32], DeST [33], IES-VE [34]) NVP assessments can account for building design elements (building simulation, Table 1) including impacts such as the internal heat gain, building envelope, occupancy schedule and

* Corresponding author.

E-mail address: luoz18@cardiff.ac.uk (Z. Luo).

<https://doi.org/10.1016/j.buildenv.2023.110621>

Received 1 May 2023; Received in revised form 10 July 2023; Accepted 15 July 2023

Available online 24 July 2023

0360-1323/© 2023 The Authors. Published by Elsevier Ltd. This is an open access article under the CC BY license (<http://creativecommons.org/licenses/by/4.0/>).

Nomenclature	
A	Effective opening area (m ²)
C _d	Discharge coefficient of opening
C _p	Wind pressure coefficient
g	Gravitational acceleration (m s ⁻²)
h _{opening}	Height of opening (m)
P _w	Wind pressure (Pa)
Q _{saving}	Cooling energy saving (J)
T	Air temperature (°C)
U	Wind speed (m s ⁻¹)
V	Ventilation rate (m ³ s ⁻¹)
α	Wind profile exponent
δ	Height where a constant mean gradient wind speed is assumed to occur (m)
λ _p	Plan area fraction
ρ ₀	Outdoor air density (kg m ⁻³)
Subscripts	
b	Buoyancy-driven
w	Wind-driven
ref	Reference condition at the meteorological station

ventilation pattern. In comparison to climate-based approaches, building simulations can mitigate uncertainties arising from building location and design. Numerous studies [35–39] have demonstrated the capability of building energy simulation tools to accurately model indoor thermal environments (hourly biases <10% for energy consumption and <1.5 °C for indoor air temperature), given that detailed and precise input data are available. Therefore, it is crucial to use appropriate weather data

inputs for building energy simulation purposes [40].

Originally (and typically) building energy simulation tools treat buildings as being isolated, using weather data input acquired from meteorological stations located in open country. However, the climate in urban areas is known to differ from surrounding rural areas due to various aspects of the urban environment potentially affecting natural ventilation [41], as shown in Fig. 1. Under wind-driven ventilation conditions the airflow pattern is influenced by surrounding buildings modifying the wind pressure on building facades [42–44]. Whilst buoyancy-driven ventilation is affected by warmer outdoor air temperatures caused by the canopy layer urban heat island effect [45], which is a result of the building fabric affecting heat storage and waterproofing [46,47], anthropogenic heat release from human activities [48,49], trapped longwave radiation [50] and reduced wind speed [45].

Considering these impacts, employing a traditional approach that relies on rural weather data for building simulations in urban environments can introduce large biases in building energy performance, indoor thermal environment and natural ventilation rate. Previous studies explored these biases resulting from neglecting the impacts of urban factors. Neglecting increases in urban air temperature can cause biases of up to 11% in building energy consumption [51–54]. For buildings situated in dense neighbourhoods (with a building plan area fraction (λ_p) of 0.6), neglecting the wind sheltering effect can overpredict the natural ventilation rate by as much as 19% [55], while overlooking the effect of inter-building longwave radiative exchange can underpredict the annual cooling energy by up to 17% [50]. Such biases in natural ventilation rates and indoor thermal environments can influence the NVP assessment.

Some studies have accounted for urban climate when assessing NVP, with most using computational fluid dynamic (CFD) models (Table 1) to obtain urban air flow and wind pressure on building facades [56]. However, CFD methods are dependent on the meteorological boundary conditions and the building morphology details, and their high

Table 1

Summary of studies on natural ventilation potential (NVP) by date. Weather data source: open - standard rural meteorological station; urban - on-site observation or CFD modelling. NVP Metric: NV-hours - natural ventilation hours; PDPH - pressure difference Pascal hours; NVCE - natural ventilation cooling effectiveness [6], ratio of actual ventilation heat loss rate to required ventilation heat loss rate. NV criteria: T - air temperature, U - wind; RH - relative humidity. Method of NVP calculation: OutMet - outdoor meteorological data, BS - Building simulation, OulnMet - Outdoor/indoor data analysis.

City Location	NVP Method	Effective NV criteria				BS tool	Weather data	NVP Metric	Urban Met	Reference
		T	U	RH	Others					
Townsville, Australia	OutMet	✓	✓	✓		–	Open	Number of occasions		[7]
Multiple China	BS	✓	✓			Own model	Open	PDPH		[8]
Athens, Greece	OutMet	✓	✓		Noise, pollution	–	Urban	No metrics - Method development	T, U	[9]
Multiple China	BS	✓	✓			Own model	Open	NV-hours, PDPH		[5]
Basel, Switzerland	OulnMet	✓	✓		Noise, pollution	–	Urban	NV-hours	T, U	[10]
Multiple China	BS	✓				Own model	Open	NV-hours		[11]
Multiple China	BS	✓	✓	✓		Own model	Open	NV-hours		[12]
Vejle, Denmark	BS	✓				EnergyPlus	Open	NV-hours		[13]
Multiple Europe	OulnMet	✓	✓			–	Open	NV-hours		[14]
Multiple China	BS	✓		✓		DeST and CFD	Urban	Mean ventilation rate	T, RH	[15]
Multiple India	BS	✓	✓			TRNSYS	Open	PDPH		[16]
Multiple US	BS	✓				EnergyPlus	Open	Target air change rate		[17]
State College, US	BS	✓	✓			IES-VE	Open	NV-hours		[18]
Multiple Global	OutMet	✓		✓		–	Open	NV-hours		[19]
Multiple China	BS	✓		✓	Pollution	EnergyPlus	Open	NV-hours		[20]
Multiple US	OutMet	✓	✓	✓		–	Urban	NV-hours	T, U, RH	[21]
Multiple Europe	BS	✓			Pollution	EnergyPlus	Open	NV-hours		[22]
Multiple Global	OutMet	✓	✓			–	Open	NV-hours		[23]
Multiple Australia	BS	✓				TRNSYS	Open	NV-hours		[24]
Multiple Spain	BS	✓		✓		DesignBuilder	Open	NV-hours		[25]
Multiple North America	BS	✓				Own model + CFD	Open	NV-hours		[26]
Boston, US	BS	✓	✓			Own model + CFD	Urban	NV-hours	T, U	[27]
Multiple China	BS	✓				EnergyPlus	Open	NV-hours		[28]
Chongqing, China	BS	✓			Pollution	EnergyPlus + CFD	Urban	NV-hours	T	[29]
Multiple US	BS	✓	✓			EnergyPlus	Open	NVE		[6]
Chambéry, France	BS	✓	✓			EnergyPlus	Open	NV-hours		[30]

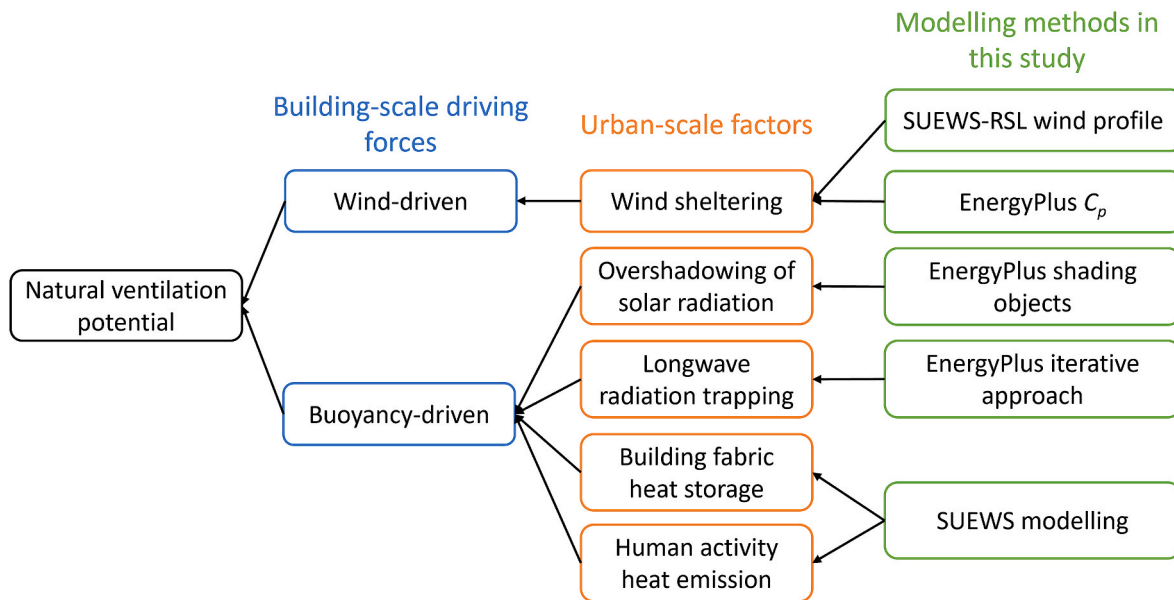


Fig. 1. Factors influencing natural ventilation potential in urban areas and the modelling methods used in this study. C_p : wind pressure coefficient.

computational costs make them unsuitable for long-term and large-scale simulations. Long-term modelling using EnergyPlus has accounted for urban climate, by modifying weather data using a simple urban heat island scenario that considers the air temperature only, so natural ventilation cooling energy savings can be simulated [57]. However, their urban heat island (UHI) prediction only considers a fixed UHI magnitude, which does not account for neighbourhood density (or building plan area fraction), and thus may not fully represent the local climate [21]. Tong et al. [21] accounted for local atmospheric conditions on NVP for super high-rise buildings using Monin-Obukhov similarity theory (MOST) approach. However, MOST applies in the inertial sublayer (a layer that begins 2 to 5 times above the mean canopy height) if present but not in the roughness sublayer [58,59]. Also, the analysis did not consider inter-buildings impacts such as radiation. In summary, the comprehensive consideration of all urban impacts shown in Fig. 1 when assessing NVP is currently limited in the existing literature.

To better account for urban impacts on NVP, in this study we propose a multi-scale modelling scheme by combining the urban land surface model: Surface Urban Energy and Water Balance Scheme (SUEWS) [60] and the building simulation tool: EnergyPlus [31].

SUEWS uses commonly available surface characteristics and climate forcing data to simulate energy and water fluxes and derive local-scale environmental parameters [60,61]. It addresses the limitations of previous urban land surface models [62,63] by specifically addressing the better representation of latent heat flux and incorporating multiple sub-models to enhance accuracy [60]. The performance of SUEWS has been extensively evaluated in diverse global climates (see Table 3 of [64]; Table 1 of [65]), demonstrating its acceptable accuracy. Notably, Tang et al. [66] evaluated SUEWS air temperature profile against observations at a central London site, considering two different heights above ground, and reported mean absolute errors (MAEs) of less than 1 °C. Furthermore, Theeuwes et al. [59] compared the wind profile modelled with the modified MOST approach embedded in SUEWS with observations in Basel and Gothenburg, reporting MAEs ranging from 0.15 to 0.5 m s⁻¹ at roof level. Applications of SUEWS in various urban environments worldwide have provided valuable insights. Researchers have used SUEWS to investigate the impacts of urbanisation on local climate (e.g. Refs. [67–69]) and building energy performance [66], assess the performance of green infrastructure (e.g. Refs. [70,71]), and analyse the effectiveness of different heat mitigation strategies (e.g. Refs. [72,73]).

The open-source U.S. Department of Energy [31] EnergyPlus building energy simulation tool is one of the most widely used, and can be used for assessing natural ventilation potential (Table 1). Following extensive evaluation, EnergyPlus has been shown to accurately model the indoor thermal environment and natural ventilation given accurate and detailed input information. For example, Royapoor and Roskilly [38] reported a calibrated EnergyPlus model can predict annual hourly indoor air temperatures with an accuracy of ± 1 °C for 93.2% of the time. Whilst, from comparing EnergyPlus Airflow Network (AFN) model results to experimental data Johnson et al. [74] conclude the model errors are generally below 30%, which is deemed acceptable for analytical natural ventilation models [75]. Notably, for buoyancy-driven cross ventilation, the error falls below 10%. Although these errors are higher than for CFD modelling (less than 10% in neutral condition, i.e. no temperature variability [76]), the advantages of AFN lie in having a better balance between accuracy and computational cost.

The SUEWS-EnergyPlus multiscale modelling scheme brings several advantages compared to previous studies. First, both models have undergone rigorous evaluations, ensuring their reliability and accuracy. Second, SUEWS has a modified MOST model [59,66,77] providing vertical profiles within the roughness sublayer (RSL) of temperature, wind, and relative humidity for where the buildings are located. Third, the scheme takes into account the impact of wind sheltering effects by incorporating local wind profiles and correspondingly modified wind pressure coefficient data [55]. Fourth, the scheme considers the influence of inter-building longwave radiative exchanges [50]. With all combined (also shown in Fig. 1), they create an effective, comprehensive multiscale modelling approach.

The objectives of this study are to: (1) improve EnergyPlus's ability to predict NVP in the urban environment, (2) analyse impacts of urban climate on the NVP, and (3) investigate how NVP changes with neighbourhood plan area fraction of buildings and climate.

2. Methods

To study the impact of urban climate on building natural ventilation potential (NVP), we couple the local-scale land surface model Surface Urban Energy and Water Balance Scheme (SUEWS) v2021a (SuPy v2021.11.20) [60,61,65,66,78] and the building energy simulation tool EnergyPlus v9.4 [31]. Representative cities from five different climate zones in China are selected to consider the climate variations.

2.1. Urban neighbourhood scale climate modelling

The urban surroundings could affect the natural ventilation of a building of interest (Fig. 2) in multiple ways (Fig. 1) by directly impacting the driving potential of NV (buoyancy force and wind-driven force). Specifically, the urban neighbourhood morphology can result in a decrease in wind speed, leading to a reduction in wind-driven natural ventilation rate. The canopy layer urban heat island (UHI) can lead to smaller temperature differences between indoor and outdoor air, which can reduce the buoyancy-driven natural ventilation rate. Here we use an urban neighbourhood wind profile, which requires the use of modified wind pressure coefficients based on differences between free-stream and urban neighbourhood wind profiles in EnergyPlus [55].

SUEWS is used to model three idealised neighbourhoods (Fig. 2) that have different building plan area densities but the same initial climate forcing data. The simulated energy and water balance fluxes are used to diagnose local-scale meteorological variables for the three neighbourhoods which are provided to EnergyPlus as the weather data for the building energy simulations. SUEWS performance has been extensively evaluated and applied in different climates globally (e.g. Table 3 of [64]; Table 1 of [65]).

SUEWS allow each neighbourhood to have varying amounts of seven land cover types: paved, buildings, deciduous trees/shrubs, evergreen trees/shrubs, grass, bare soil and water. This allows realistic intra-city land cover variations, between different cities. For simplicity, here we assume neighbourhoods consist of buildings and grass (i.e., two typical but contrasting surface types), so vegetation's influence (e.g., evapotranspiration) is considered but more complicated impacts, such as trees/shrubs influence on wind [79] and radiation [80] are not included. Our three neighbourhoods are:

- rural* (Fig. 2a): is a large area covered with 100% grass, hence the isolated building area is negligible
- medium density* (Fig. 2b): has buildings covering 30% of the area (plan area fraction $\lambda_p = 0.3$) and grass covering 70%
- high density* (Fig. 2c): has $\lambda_p = 0.6$ and grass in the remaining 40% of the area

The SUEWS neighbourhood population density is consistent with the EnergyPlus building occupancy (Section 2.2).

The Design Standard for Energy Efficiency of Public Buildings [81] classifies China into five climate zones (Table 2) using typical average air temperatures in January and July as the primary indicators. This classification aims to provide guidance on the design of building envelope thermal characteristics for each specific climate zone and identifies the major cities in the zone. Here we use the ERA5 (ECMWF Reanalysis version 5) [82] meteorological data, which are available globally at a spatial resolution of 0.125° and a temporal resolution of a hour. As natural ventilation cooling for buildings is particularly important during hot periods, we select 2018, the year with the warmest Northeast Asia summer (JJA) mean near-surface air temperature between 1979 and 2018 [83] for simulation. The three neighbourhoods are simulated in

one city for each of the five climates (Table 2), assuming human activities do not vary between the regions. One ERA5 grid located in centre of the city is used. Note the ERA5 data do not account for urban land cover in the reanalysis but do assimilate meteorological data with cities [66]. The vegetation cover assigned to the grid is representative of local conditions [82].

To drive SUEWS the meteorological data in the inertial sub-layer or constant flux layer are needed. This layer is located above the roughness sub-layer (RSL). Within the RSL individual roughness element influences the air flow, while above that the flow becomes blended and provides a neighbourhood or local scale response. The RSL extends from ground to a depth of approximate 2 to 5 times of mean roughness element height (i.e. buildings and trees) [84], where the buildings are located and most human activities occur. Thus, SUEWS forcing height depends on both the building height (i.e. height above ground level) and the city altitude (height above sea level, see Fig. 1 in [66]). With a mean building height of 6.4 m (Fig. 2) the forcing height above ground level (agl) needs to be at least 12.8–32 m agl. For example, central Kunming is located at an altitude of 1892 m above sea level (asl) [85], whereas the larger ERA5 grid-cell over central Kunming has an altitude of 2000 m asl (or 108 m agl). Therefore for Kunming a forcing height of 108 m agl is used. For climates with ERA5 height less than 32 m agl, the ERA5 data are adjusted to the appropriate height using the environmental lapse rate following Appendix B in [66].

Building energy simulation of natural ventilation potential, requires wind speed U , air temperature T and relative humidity RH in the RSL. Here we use the SUEWS-RSL module to obtain the environmental variables. SUEWS-RSL calculates vertical profiles of these variables with a RSL using the corrected MOST (Monin-Obukhov Similarity Theory) approach [59,77,86], while accounting for varying atmospheric stability, roughness characteristics and turbulent heat fluxes [59,66]. Evaluation of the SUEWS-RSL U and T profiles against observations in three global cities, suggests an acceptable accuracy [59,66].

The SUEWS-RSL generates local weather data, includes T and RH at 2 m above ground (T_2 and RH_2), U at 10 m (U_{10}), and vertical profiles of T and U within the RSL (Fig. 3). The supplied T_2 , RH_2 and U_{10} as well as other climate data (e.g., incoming solar radiation from ERA5) are formatted as an EnergyPlus weather file (.epw). The SUEWS-RSL wind profile is passed to EnergyPlus via input files (.idf) by replacing the power law coefficients with values derived from the SUEWS-RSL data.

In EnergyPlus solar shading from adjacent buildings (purple, Fig. 2) are simulated as 'shading objects'. The longwave radiative exchanges between the reference building and adjacent buildings are calculated with an iterative approach [50]. Impacts of other urban factors like the heat storage and the anthropogenic heat are simulated with SUEWS and accounted for in the outdoor air temperature calculation (Fig. 1 and 3).

2.2. Building characteristics

To compare the NVP, a two-storey building model (Fig. 2a) based on ASHRAE Case 600 [87] is developed in EnergyPlus. The 8 m wide \times 8 m long \times 6.4 m tall, building has no interior partitions. There are two

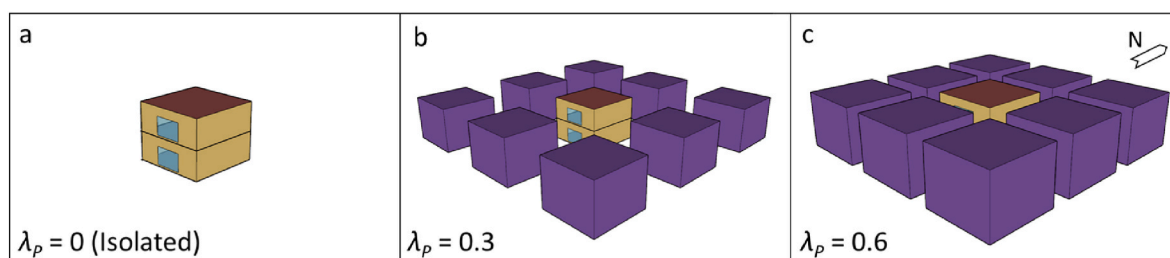
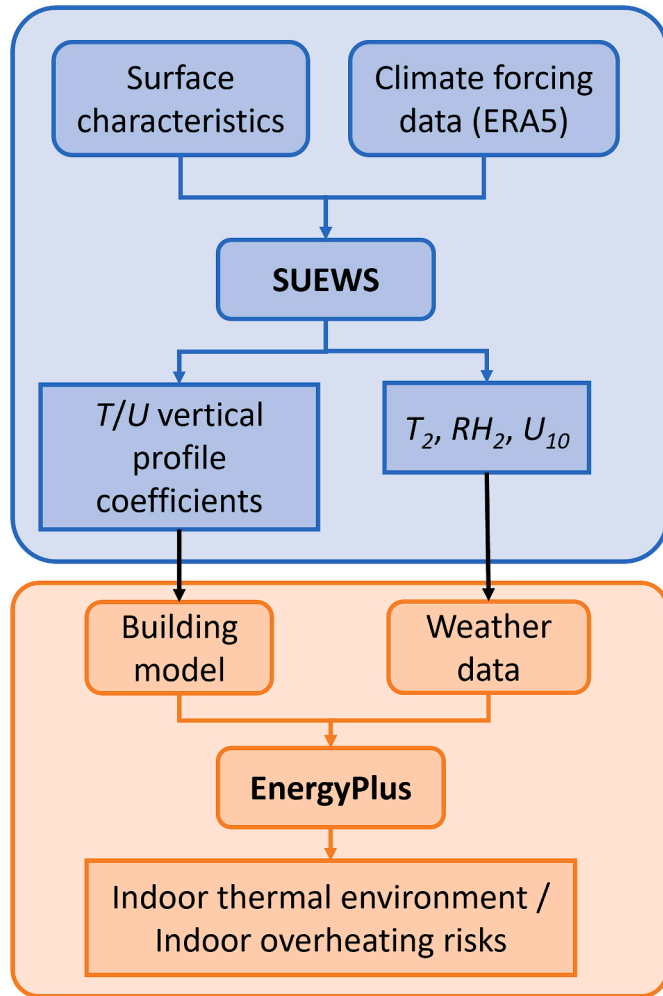


Fig. 2. Reference building (8 m \times 8 m \times 6.4 m) is simulated (EnergyPlus) after the weather data is simulated (SUEWS) for three neighbourhoods: (a) a rural (isolated), and two city neighbourhoods with building plan area fractions (λ_p) of (b) 0.3 and (c) 0.6.

Table 2

Building thermal characteristics and specific city simulated in each climate zones in China. SHGC: solar heat gain coefficient. Modified from Ref. [20].

City	Climate zone	U-value ($\text{W m}^{-2} \text{K}^{-1}$)				SHGC
		Roof	External wall	Ground floor	Window	Window
Harbin	Very cold	0.25	0.35	0.25	1.76	0.68
Beijing	Cold	0.39	0.46	0.46	1.77	0.37
Shanghai	Cold winter hot summer	0.39	0.54	0.46	2.3	0.32
Kunming	Temperate	0.44	0.72	1.32	2.4	0.2
Guangzhou	Warm winter hot summer	0.44	0.72	1.32	2.4	0.2

**Fig. 3.** Overview of the SUEWS-EnergyPlus workflow integration [66].

windows on each floor, one on the south-facing and one on the north-facing wall to provide natural ventilation. All four windows are $2 \text{ m} \times 3 \text{ m}$. A simplified residential occupancy (2 people on each floor, $125.6 \text{ W person}^{-1}$, occupied all-day) and internal heat gain (lighting: 6 W m^{-2} , equipment: 4.3 W m^{-2}) are assumed [88]. The simulated reference building is assigned the Design Standard for Energy Efficiency of Public Buildings [81] thermal characteristics appropriate for each climate zone (Table 2).

For the NVP analysis, we consider both cross and single-sided ventilation (only south-facing windows are open). All windows are assumed to have 15% openable area and discharge coefficient (C_d) of 0.61. For the cooling energy savings calculation, an ideal load system is assumed with a heating setpoint of 18°C and cooling setpoint of 26°C based on the recommendation of the Code for Thermal Design of Civil Building [89].

2.3. Natural ventilation models

To simulate the cross ventilation the Airflow Network (AFN) model within EnergyPlus is used [90]. The AFN has been evaluated and widely used for natural ventilation calculations [74]. The AFN airflow rate is calculated using the pressure difference across openings, with the standard orifice flow equation. The wind-driven ventilation rate V_w is [91]:

$$V_w = C_d A \sqrt{\frac{2\Delta P_w}{\rho_0}} \quad (1)$$

where C_d is the discharge coefficient of opening, A is the effective opening area (m^2), ρ_0 is the outdoor air density (kg m^{-3}) and ΔP_w is the wind pressure difference across opening (Pa). The wind pressure at the opening height is [91]:

$$P_w = 0.5\rho_0 C_p U_{free}^2 \quad (2)$$

where C_p is the surface-averaged wind pressure coefficient, and U_{free} is the upstream undisturbed flow at the opening height.

As C_p values are influenced by the building geometry, surrounding conditions and wind profile and direction [92], it is important to use the appropriate C_p values as it impacts the accuracy of the building natural ventilation simulation in an urban environment. In this study, TPU *Aerodynamic Database of Non-isolated Low-Rise Buildings* [93] C_p data from wind-tunnel experiments for buildings with different geometries and surrounding conditions are used. As the TPU C_p database is for free-stream wind measured in wind tunnel experiments, we modified these using the SUEWS-RSL wind speeds and profile as shown in Ref. [55].

Although it is widely accepted that cross ventilation usually achieves much larger ventilation rate, it is less practical than single-sided ventilation for urban buildings where isolated rooms are common [94]. The single-sided ventilation model, based on the mixing layer theory [95, 96], is used. This has been evaluated in wind-tunnel and full scale experiments [97,98]. The wind-driven ventilation rate (V_w , $\text{m}^3 \text{ s}^{-1}$) is calculated with:

$$V_w = 0.1AU \quad (3)$$

From Bernoulli principles, the buoyancy-driven ventilation rate (V_b) is calculated with:

$$V_b = \frac{C_d A}{3} \sqrt{gh_{opening} \frac{\Delta T}{T}} \quad (4)$$

where g is the gravitational acceleration, $h_{opening}$ the height of the opening, ΔT air temperature difference across the opening. The total ventilation rate (V_t) is the quadrature sum of the wind and stack air flow components [99]:

$$V_t = \sqrt{V_w^2 + V_b^2} \quad (5)$$

2.4. Analysis metrics

In this study, the natural ventilation hours (NV-hour) and the

cumulative air change rate (ACH-hour) are used to quantify the natural ventilation potential (NVP).

The NV-hour, the most common NVP metric (Table 1), is the number of hours per year when natural ventilation can fulfil both the air quality and thermal comfort requirements [5,12]. ASHRAE Standard 62.1 [100] defines the required minimum outdoor airflow rate (V_R) for a residential space as a function of the number of people occupying (N_p) the floor area (A_f , units: m^2) as:

$$V_R = 0.0025N_p + 0.0003A_f \quad (6)$$

In this study, as each floor has $N_p = 2$ and $A_f = 64 m^2$, $V_R = 0.0242 m^3 s^{-1}$ (≈ 0.425 ACH).

For free-running building thermal comfort assessment, we use the Chinese adaptive thermal comfort models provided in the *Evaluation Standard for Indoor Thermal Environment in Civil Buildings* [101] for 75% satisfaction (or Category II). These specify an upper (T_{UL}) and lower indoor operative temperature limit (T_{LL}) by zone, with the northern (very cold, cold, Table 2):

$$\begin{cases} T_{UL,N} = 0.73T_{rm} + 15.28 & (18^\circ C \leq T_{UL,N} \leq 30^\circ C) \\ T_{LL,N} = 0.91T_{rm} - 0.48 & (16^\circ C \leq T_{LL,N} \leq 28^\circ C) \end{cases} \quad (7)$$

and southern zones (cold winter hot summer, temperate, warm winter hot summer, Table 2):

$$\begin{cases} T_{UL,S} = 0.73T_{rm} + 12.72 & (18^\circ C \leq T_{UL,S} \leq 30^\circ C) \\ T_{LL,S} = 0.91T_{rm} - 3.69 & (16^\circ C \leq T_{LL,S} \leq 28^\circ C) \end{cases} \quad (8)$$

This uses a seven day ($n = 7$) running mean of the outdoor air temperature (T_{rm}):

$$T_{rm} = (1 - k)(T_{od-n} + \alpha T_{od-n-1} + \alpha^2 T_{od-n-2} + \dots + \alpha^6 T_{od-n-7}) \quad (9)$$

where k is a constant between 0 and 1, with 0.8 recommended [102], and T_{od-n} is the daily mean outdoor air temperature for n days ago ($^\circ C$).

As higher ventilation rates may prevent sick building syndrome symptoms and reduce potential airborne infection risk [103], we also determine the ACH-hour, or cumulative air change rate during the NV-hour period. This is similar to pressure difference Pascal hours (PDPH) [8]. Although both aim to quantify availability of natural driving forces, ACH-hour is more directly linked to amount of ventilation.

Cooling energy saving (Q_{saving}) is also determined [20]:

$$Q_{saving} = Q_{window_closed} - Q_{window_open} \quad (10)$$

The is the difference in energy demand between a fully air-conditioned building (i.e. windows always closed, Q_{window_closed}) and a hybrid-controlled building with windows open (Q_{window_open}) when the indoor air temperature can vary between the heating and cooling set points ($18\text{--}26^\circ C$) while the air conditioning system is turned off. The air-conditioning system setting are given in Section 2.1.

In summary (Fig. 4), three metrics are determined from analysis of simulations for five climates and for three neighbourhoods with

different plan area fractions (λ_p) and two ventilation types. Thus, a total of ($5 \times 3 \times 2 =$) 30 cases are simulated.

We use the mean bias error (MBE) to assess the difference between SUEWS-RSL and modified EnergyPlus wind profiles (Eq. (12), Table 3 coefficients):

$$MBE = \frac{1}{N} \sum_{i=1}^N (y_i - x_i) \quad (11)$$

where y_i and x_j are EnergyPlus and SUEWS-RSL wind speeds at each timestep, and N is the number of values analysed (i.e. a year with hourly timestep, $N = 8760$).

3. Results

3.1. Outdoor climate

First, we assess differences in modelled local environmental variables for the neighbourhoods with different building plan area fractions (λ_p) and in different climate zones (Fig. 4).

Modelled outdoor air temperature at 2 m (T_2) in denser neighbourhoods (larger λ_p , green Fig. 5) have warmer monthly values and greater variation than that at the rural site in all five climates (blue, Fig. 5). Annual mean differences in T_2 between cases with λ_p of 0.6 and 0 vary between $0.8^\circ C$ in Guangzhou and $1.6^\circ C$ in Kunming. This difference is indicative of the canopy layer urban heat island effect.

Whereas the monthly variation of SUEWS-RWL modelled wind speed at 10 m (U_{10}) decrease as λ_p increases (Fig. 6). The annual mean differences ($\Delta \lambda_p 0.6 \rightarrow 0$) are the smallest in Beijing ($0.6 m s^{-1}$) and the largest in Harbin ($1.1 m s^{-1}$). These results are qualitatively similar to previous CFD studies considering outdoor velocity and λ_p (e.g. [104]).

Vertical wind profiles (Fig. 7) derived SUEWS-RSL are used to calculate the EnergyPlus power-law parameters (δ, α , Table 3) [105]:

$$U_z = U_{10} \left(\frac{\delta_{ref}}{10} \right)^{\alpha_{ref}} \left(\frac{z}{\delta} \right)^\alpha \quad (12)$$

where the meteorological station boundary layer depth (δ_{ref}) and exponent (α_{ref}) are obtained as the default settings in EnergyPlus for open terrain [106].

To assess the mean bias error (MBE) for the EnergyPlus wind profiles when using Table 3 coefficients (hereafter EP-RSL profiles), we use the original SUEWS-RSL vertical wind profiles data which vary because of the different forcing heights; (5–8 vertical levels for $\lambda_p = 0$; 9 levels at $\lambda_p = 0.3$ and 0.6) as the baseline (Fig. 8). As the SUEWS-RSL wind profile does not assume a power law and varies with stability [59,66], biases still exist in EP-RSL profiles. The biases are larger for climates with stronger wind speeds (e.g. Harbin). When $\lambda_p = 0$, the EP-RSL profiles underpredicts the median wind speeds by up to $0.35 m s^{-1}$, especially around 2 m above ground level. For $\lambda_p = 0.3$ the EP-RSL MBE_{median} are smaller ($\leq 0.2 m s^{-1}$), as are $\lambda_p = 0.6$ cases. As the MBE_{median} become better (smaller) with height within the canopy layer ($>3.2 m$), we focus analysis on the upper floor natural ventilation potential and energy

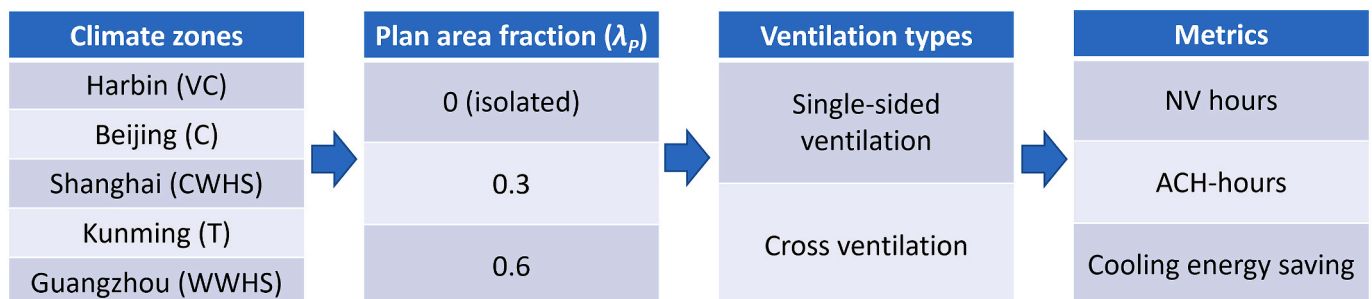


Fig. 4. Variables and metrics analysed in this study. See Fig. 2 and Table 2 for more details.

Table 3

Wind power law (Eq. (12)) coefficients derived from SUEWS-RSL model output for each climate and neighbourhood.

λ_p	Exponent α					Boundary layer depth δ (m)				
	Harbin (VC)	Beijing (C)	Shanghai (CWHS)	Kunming (T)	Guangzhou (WWHS)	Harbin (VC)	Beijing (C)	Shanghai (CWHS)	Kunming (T)	Guangzhou (WWHS)
0	0.31	0.28	0.31	0.27	0.28	40.41	37.88	37.34	46.62	46.93
0.3	0.16	0.25	0.17	0.22	0.17	380.44	125.28	322.01	149.76	320.19
0.6	0.67	1.02	0.68	0.86	0.68	25.96	16.16	25.11	16.65	24.87

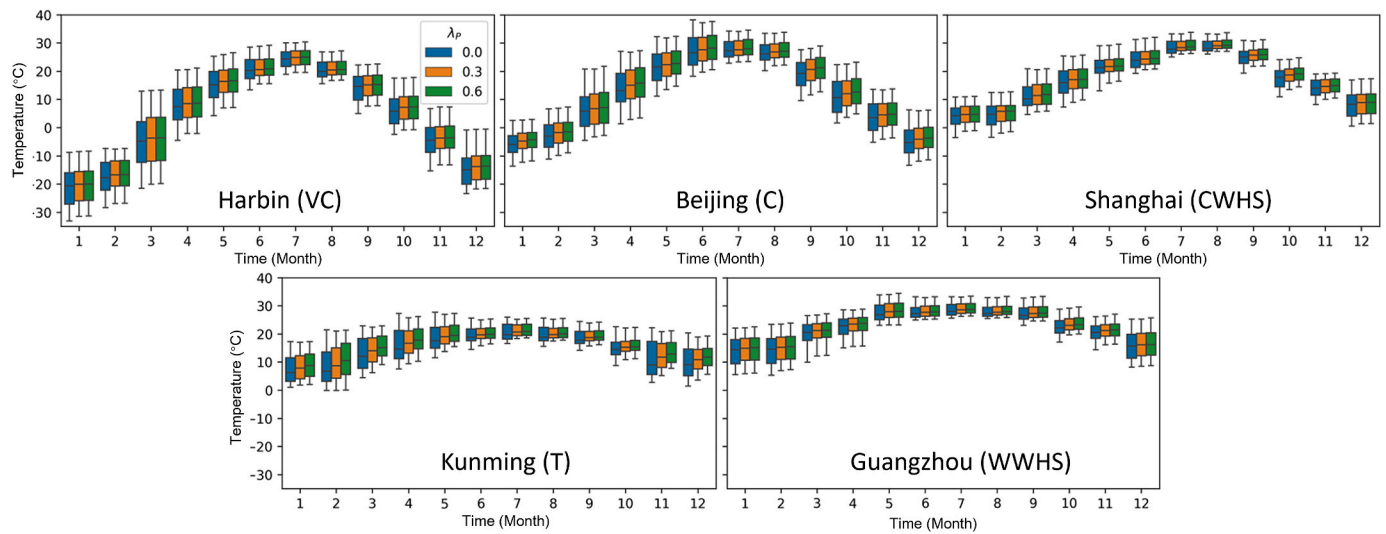


Fig. 5. Monthly distribution (hourly) of modelled outdoor air temperature at 2 m agl for three plan area fraction of buildings (λ_p , Fig. 2; colours) and five climates (Table 2), with interquartile range (box), median (horizontal line) and 5th and 95th percentiles (whiskers).

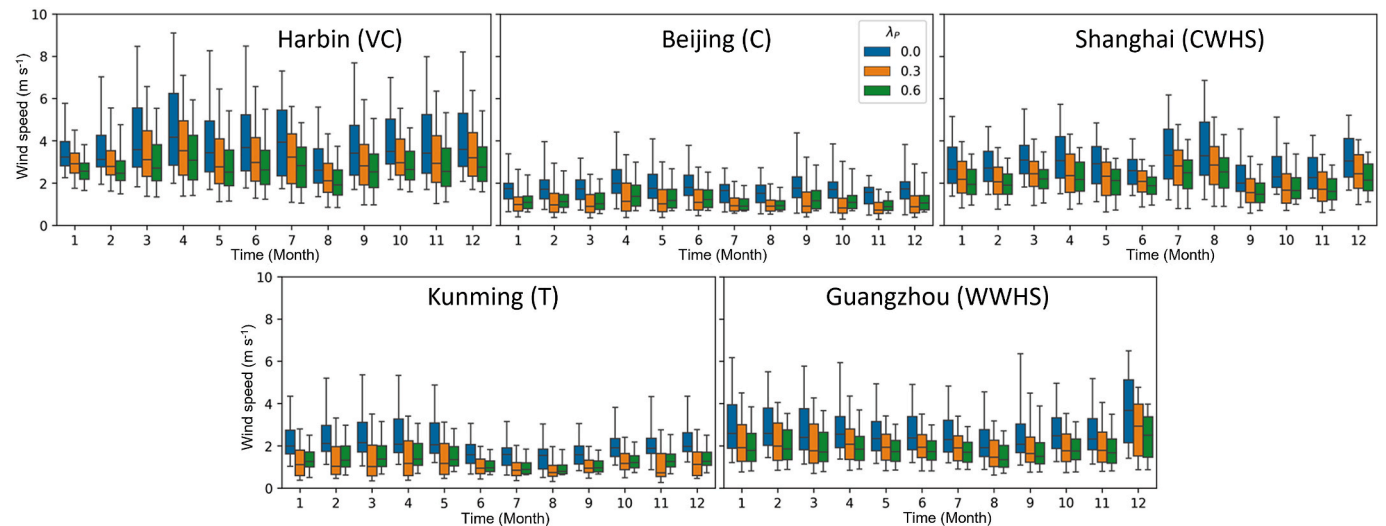


Fig. 6. As Fig. 5, but wind speed at 10 m agl.

saving. Future work could directly use the RSL wind profile within EnergyPlus after rewriting the appropriate code. This is beyond the scope of this study.

3.2. Natural ventilation potential (NVP)

3.2.1. Natural ventilation hours (NV-hour) of cross ventilation

Cross ventilation monthly percentage of NV-hours across the five climates (Table 2) and three λ_p classes (Fig. 2) are generally larger for upper floor room (Fig. 9). With windows always opened, the minimum ventilation rate requirement of 0.425 air change per hour (ACH) (section

2.4) can be fulfilled during most of the year (Fig. 9). Although the Beijing neighbourhood with $\lambda_p = 0.6$ has the lowest wind speeds, there are only 23 h within the year that do not meet the ventilation rate criteria. Thus, differences in NV-hours are mostly influenced by the thermal comfort criteria. As a result, warm climates (Guangzhou, Kunming, Shanghai) have more annual total NV-hours than cold climates (Harbin, Beijing), since there is very limited NV potential for cold climates in winter (Fig. 9).

Influences of λ_p on NV-hours vary across climates (Fig. 9). In terms of the annual total, the building in the $\lambda_p = 0$ rural neighbourhood has the most annual NV-hours in hot climates like Guangzhou. While for low-

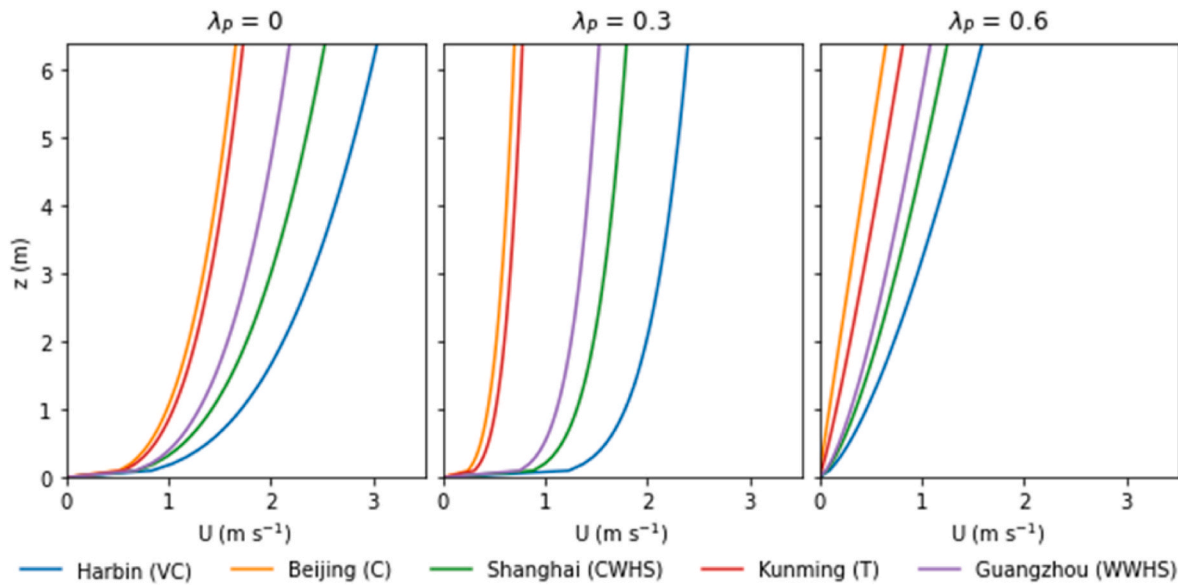


Fig. 7. Vertical wind profiles for three different λ_p and five climates (colour) calculated with annual median 10 m wind speeds and coefficients (Table 3) derived from the SUEWS-RSL results (EP_{RSL}) within the canopy layer (building height = 6.4 m).

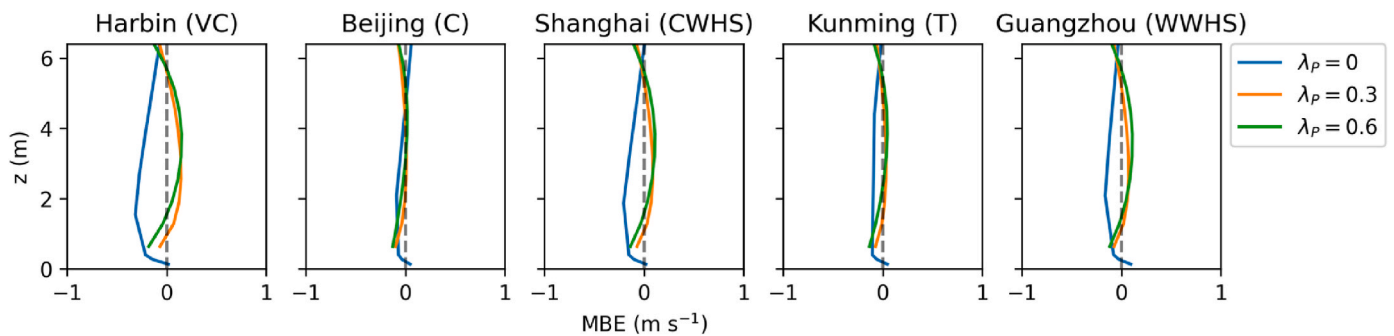


Fig. 8. Annual mean bias error (MBE) for wind speed calculated at hourly timestep but vertical resolution (Δz) that varies (from 0.13 m with varying Δz for $\lambda_p = 0$; from 0.64 m with $\Delta z = 0.64$ m for $\lambda_p = 0.3$ and 0.6) to 6 m above ground level; where SUEWS-RSL (x , Eq. (11)) and EP-RSL wind profiles (y , Eq. (11); using Eq. (12), and Table 3 coefficients) for three λ_p (colour) and five climates.

medium density $\lambda_p = 0.3$, warm winter hot summer climates like Shanghai have the most annual NV-hours. Dense urban neighbourhoods ($\lambda_p = 0.6$) have the most annual NV-hours in cold northern zones including Harbin and Beijing, and the mild climates like Kunming. This can be explained by the air temperature distribution (Fig. 6) as dense neighbourhoods ($\lambda_p = 0.6$) tend to have higher outdoor temperatures (in their regional climate), which is beneficial in cool climates for thermal comfort, and vice versa. The annual differences in NV-hours between $\lambda_p = 0$ and $\lambda_p = 0.6$ is largest in Kunming (1545). This is more than twice the difference to the next largest (Harbin, 753). The others are smaller in Guangzhou (587), Shanghai (254), and Beijing only 201 NV hours.

The λ_p has a greater impact on nocturnal NV-hours than daytime (Fig. 9), linked to the larger night-time temperature differences (Fig. 5). During cool months there are larger proportion of daytime NV-hours, but the nocturnal NV-hours increases with λ_p to a greater extent (e.g. nocturnal NV-hours increase by 33.9% while daytime increase by 13.2% from $\lambda_p = 0$ to 0.6 during March in Kunming). While in warm months, nocturnal NV-hours are reduced more with the increase of λ_p (e.g. nocturnal NV-hours decrease by 35.3% while daytime increase by 16.3% from $\lambda_p = 0$ to 0.6 during July in Guangzhou).

Generally, the dependence of NV-hours change with λ_p is highly related to climate and seasons (Fig. 10). In summer, very cold climates (e.g. Harbin) have an increase in NV-hours with λ_p (10% $\lambda_p = 0.6$ cf. $\lambda_p = 0$), while the opposite occurs in hot summer climates regions (-43% λ_p

= 0.6 cf. $\lambda_p = 0$ in Guangzhou). Whereas in the temperate climate (e.g. Kunming) λ_p has negligible impact on NV-hours, as temperatures have both small variations and are usually pleasant for indoor thermal comfort (Fig. 9). In winter, NV-hours increase with λ_p in all regions due to cooler outdoor air temperatures, but the increase is small in regions with cold winter and little natural ventilation potential including Harbin, Beijing and Shanghai. During the spring/autumn transition seasons, the NV-hours tend to increase with λ_p in most climates associated with the relatively mild outdoor climate except Guangzhou, where the warm climate causes the indoor air temperature to exceed the upper limit of thermal comfort in late spring (May) and early autumn (September) (Fig. 9).

3.2.2. ACH-hours of cross ventilation

The air exchange rates can enhance the NV benefits for air quality purposes. The annual variability in ACH (hourly) during NV period (Fig. 11) is the largest when buildings are sited in open areas ($\lambda_p = 0$) because of the higher variability of wind speed (Fig. 6 and 8), with median ACH between 10.8 (Beijing) and 20 (Harbin). As λ_p increases the median ACHs become smaller ($\lambda_p = 0.3$: 4.9 ACH (Beijing) and 10.1 ACH (Harbin); $\lambda_p = 0.6$: 2.6 ACH (Beijing) and 3.0 ACH (Harbin)).

The annual cumulative ACH-hours differs from NV-hours with λ_p variations. As ACH-hours largely depend on wind speeds and ACH-hours decrease with λ_p in all climates (Fig. 12), the inter-climate variations are

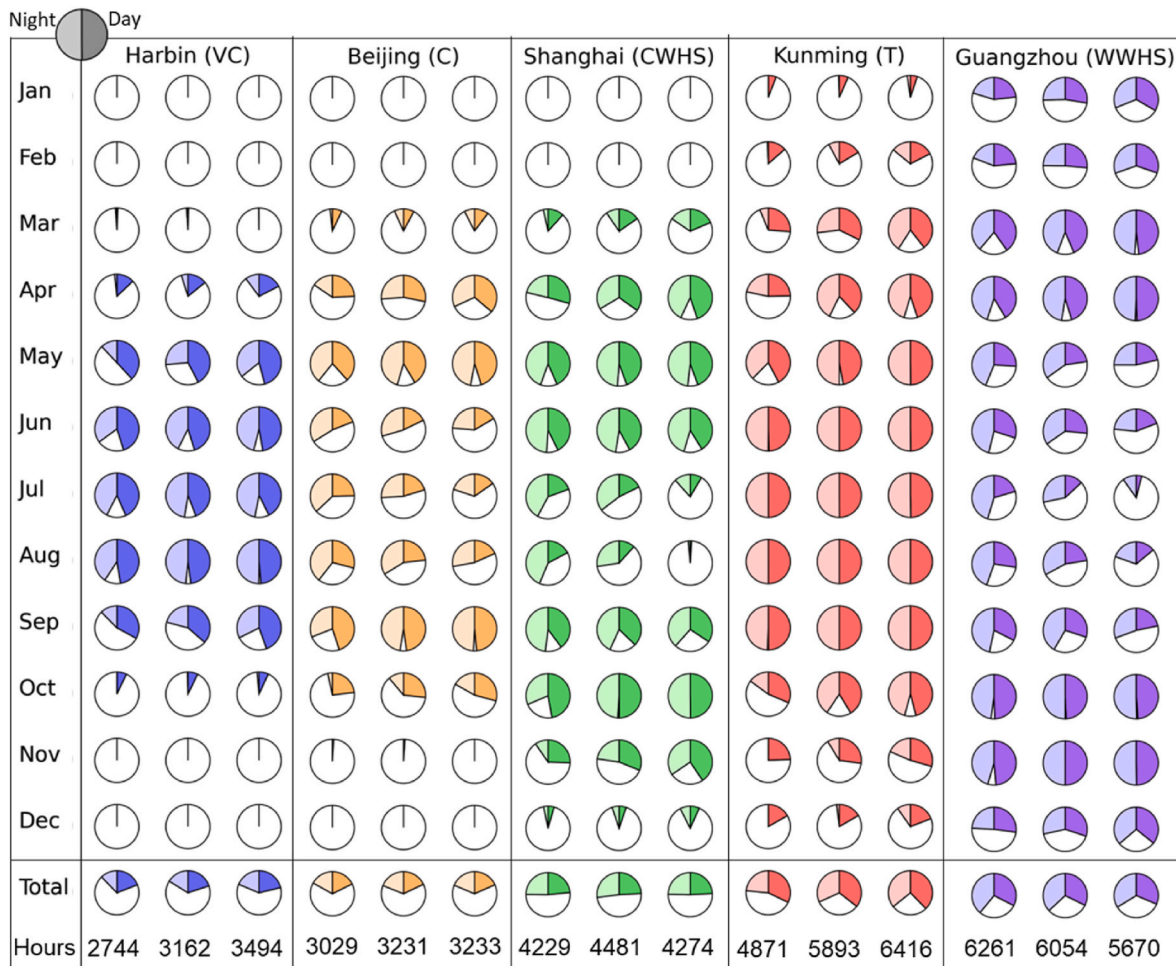


Fig. 9. Upper floor cross ventilation as percentages of NV-hours (relative to total hours in the period for five climates (columns), three neighbourhoods (λ_p , left: 0; middle: 0.3; right: 0.6) and different time intervals (rows: monthly and annual, time of day (pie chart half): right daytime (7:00 to 19:00), left night-time (19:00 to 7:00)).

smaller (Fig. 12). Given the large number of annual NV-hours, buildings in areas with a λ_p of 0 and 0.3 in Guangzhou and $\lambda_p = 0.6$ in Kunming have the most ACH-hours (cf. to buildings in the same λ_p neighbourhoods but different climates). While Beijing has the least annual ACH-hours for all λ_p due to low both ventilation rate and NV-hours.

The seasonal variations in ACH-hours are also influenced by both NV-hours and ventilation rates (Fig. 13). In transition seasons (spring/autumn), Guangzhou's climate has the largest ventilation potential in both ACH-hours and NV-hours (Fig. 10) benefiting from appropriate air temperatures and wind speeds, while Kunming's ranking drops due to the low ventilation rates. In summer, high wind speeds and mild summer temperatures make Harbin with the most ACH-hours. The ranking of ACH-hours in winter remains consistent with the NV-hours.

3.2.3. Single sided ventilation

To assess NVP differences between cross ventilation and single-sided ventilation we focus on Shanghai as similar conclusions are drawn for the other cities. Ventilation rates are largely less for single-sided ventilation (cf. cross ventilation) (Fig. 14) with annual median ACH reducing from 15.1/8.2/2.7 ACH (cross ventilation) to 3.9/2.9/2.1 ACH (single-sided ventilation) across the three plan area densities ($\lambda_p = 0/0.3/0.6$). This also implies that the single-sided ventilation is as effective as cross ventilation for buildings located in dense urban areas. Although the ventilation rates are reduced, the annual minimum ventilation rate for the single-sided ventilation building even for $\lambda_p = 0.6$ (0.59 ACH), still meets the requirement of indoor air quality. Therefore, in Shanghai the

natural ventilation potential is mainly influenced by thermal comfort criteria only. However, we do not consider the impact of outdoor air pollution (i.e., assuming outdoor air is unpolluted).

The reduced ventilation cooling potential with single-sided ventilation causes median indoor air temperature to increase by 0.9/0.8/0.2 °C for $\lambda_p = 0/0.3/0.6$ (Fig. 14). The seasonal percentage of NV-hours with single-sided ventilation therefore increases by up to 10.6% ($\lambda_p = 0$) during spring and autumn, but decreases by up to 14.7% ($\lambda_p = 0.3$) in summer (cf. cross ventilation) (Fig. 15). The ACH-hours are higher with cross ventilation in all conditions due to the higher ventilation rate, and differences between ventilation modes decreases as λ_p increases (Fig. 16).

Generally, the single-sided ventilation leads to lower ventilation rates across λ_p , and reduce the natural ventilation potential in magnitude. The changing pattern of NVP with λ_p is similar to cross ventilation.

3.3. Cooling energy saving

The cooling energy saving is calculated as the difference in cooling energy demand between a building with air-conditioning only and hybrid ventilation (air-conditioning plus natural ventilation). Therefore, the cooling energy saving amount is linked with the effectiveness of natural ventilation cooling (Eq. (10)). Cooling energy saving is expected to be larger for climates and neighbourhoods with lower outdoor air temperatures and higher wind speeds. Hence, in all climates the cooling energy saving decreases as λ_p increases (Fig. 17). For cross ventilation,

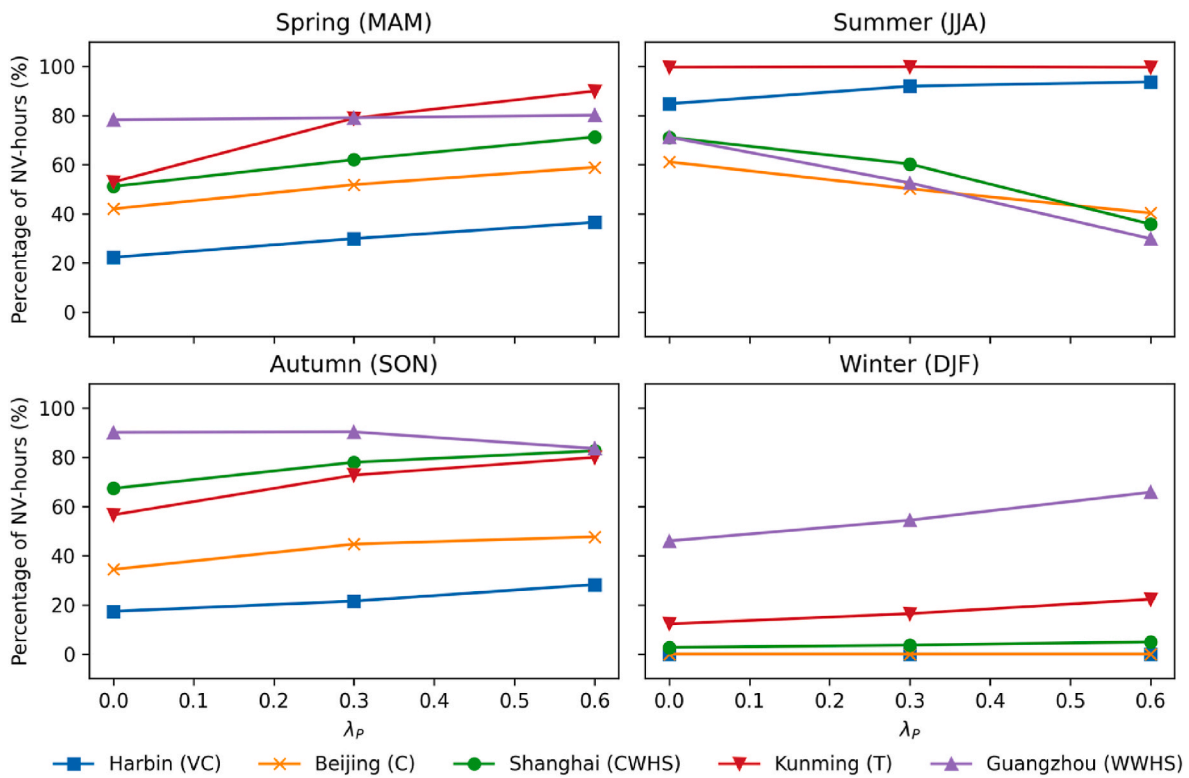


Fig. 10. Seasonal upper floor with cross ventilation (percentage of NV hours) in five climates (colour) for three λ_p (x axis).

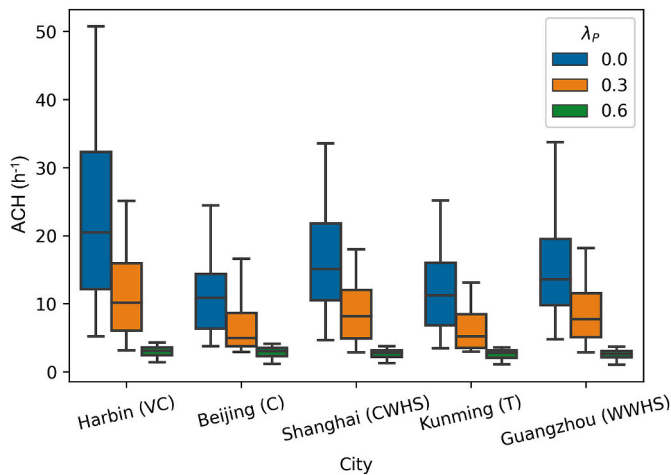


Fig. 11. Annual variability in air changes per hour (ACH) when the upper floor has cross ventilation (NV-hour >0) throughout the year for five climates and three λ_p (colours) with interquartile range (box), median (horizontal line) and 5th and 95th percentiles (whiskers).

such decreases are smallest in Kunming, as the climate is mild and temperature variation is small, making natural ventilation cooling available most of the time. For the other climates the cooling energy saving between building densities (λ_p) are similar (Harbin: 8% to Beijing: 12.5%).

Our results differ slightly from Ramponi et al's. [57]'s nocturnal ventilation cooling energy saving study of three European cities. They suggest inter- λ_p differences are largely influenced by the climate, with natural ventilation cooling energy saving dropping by 20% in cool but windy Amsterdam, while in warmer less windy Milan (2%) and Rome (13%) reductions are less. Differences may arise from their different approach, as their outdoor air temperatures and wind speeds are

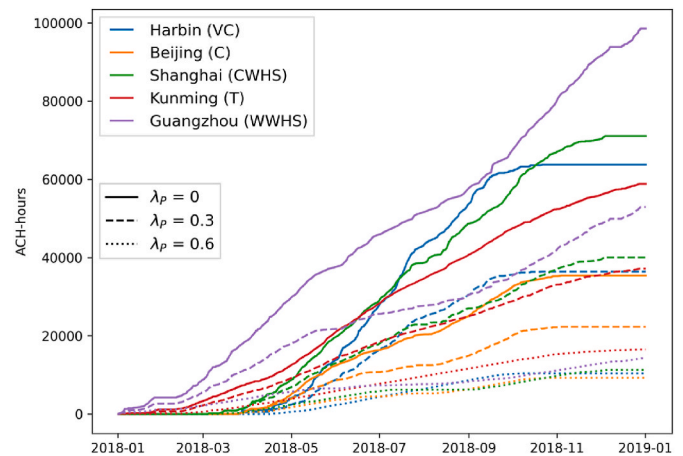


Fig. 12. Annual cumulative ACH-hours of the upper floor with cross ventilation for different climates (colour) and λ_p (line style).

independent of λ_p (only C_p values changed), and longwave radiative exchanges are not considered. The last may be critical as increased λ_p can result in more trapped longwave radiation, increasing building cooling demand [50]. Our work highlights the importance of a holistic consideration of the complex interaction between urban climate and building performance.

Compared to cross ventilation, single-sided ventilation has less cooling energy savings due to lower wind speeds. The trends across climates are similar, despite slightly smaller inter- λ_p variations (6.5%–8.1% excluding Kunming).

4. Discussion and conclusions

Although NVP across China's climate zones has been assessed previously, given the large dependence on research approach, climate data

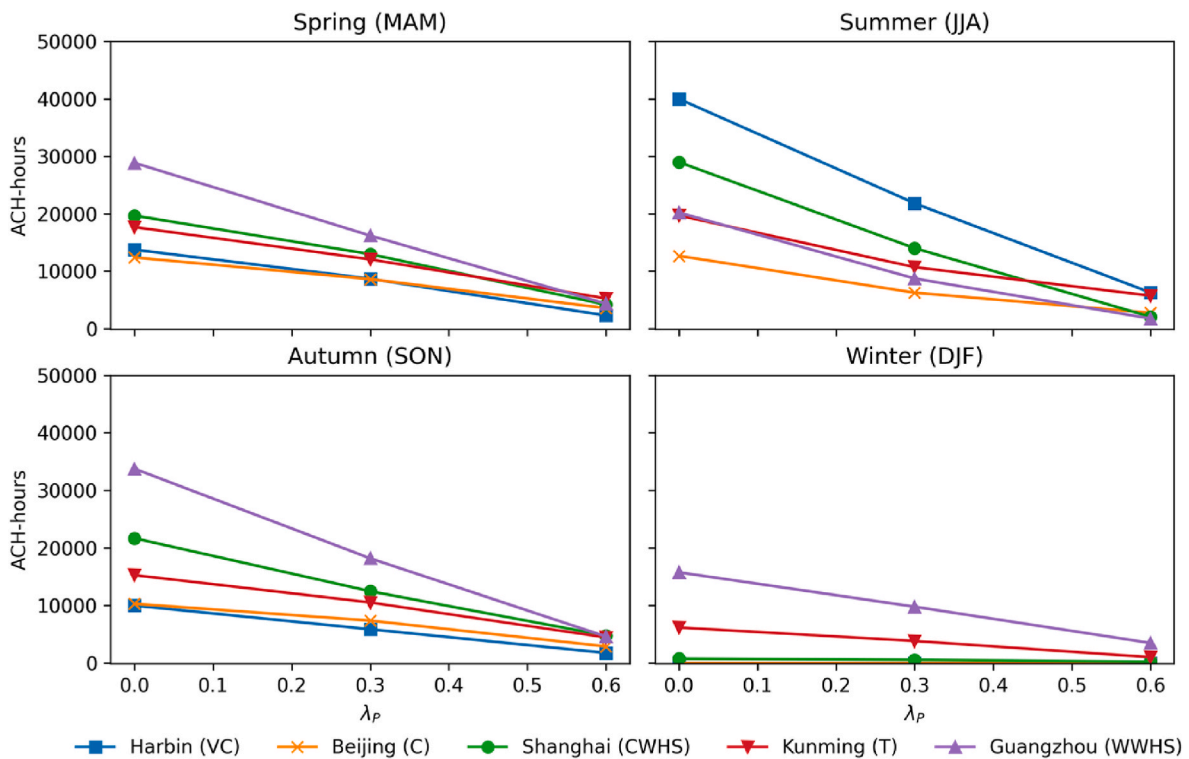


Fig. 13. Seasonal upper floor ACH-hours with cross ventilation in five climates (colour) for three $\lambda_p \times$ axis.

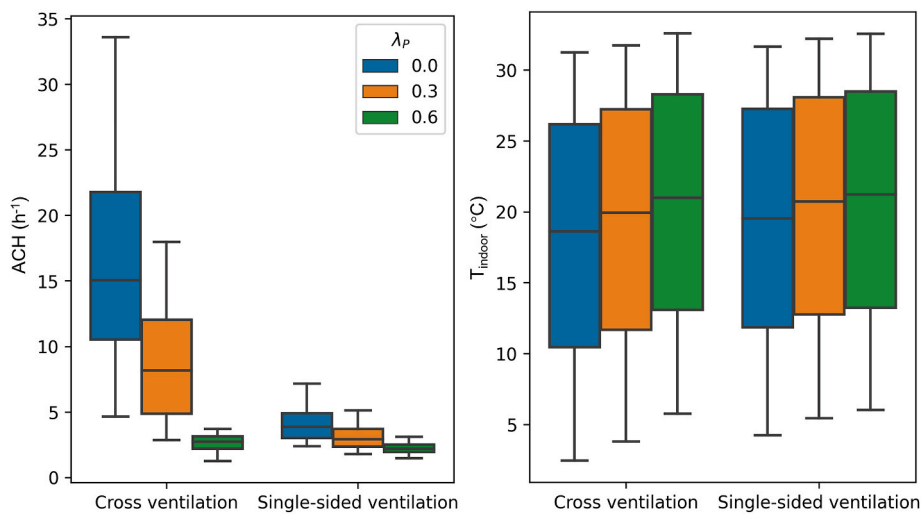


Fig. 14. Shanghai annual variability for two ventilation modes in (left) upper floor air changes per hour (ACH) and (right) indoor air temperature.

and building model used, the results vary [5,8,11,20]. However, the urban factors influencing buildings in an urban environment are often not fully considered.

In this study, we propose a multi-scale modelling scheme that combines the urban land surface model SUEWS and building energy simulation tool EnergyPlus to assess the natural ventilation potential (NVP) of buildings in different Chinese climate zones and neighbourhoods with different building plan area fractions (λ_p). Unlike traditional approaches that treat buildings as being isolated and use rural weather data, our approach considers multiple urban factors, including the influence of the urban neighbourhood morphology on canopy air temperature, wind sheltering effects, overshadowing, and longwave radiative exchanges. Compared to computationally intensive methods like CFD, our approach offers practical advantages in terms of simplicity and minimum

computational cost. The SUEWS model only requires commonly available surface characteristics and meteorological forcing data. A year long run for one neighbourhood normally takes around 1 min (PC) which is around 10^6 times less than CFD-based approaches (e.g. 3-day run taking 168 h on PC by Ref. [107]). Therefore, our approach can be applied for quick estimates of natural ventilation potential and cooling energy saving in larger scales (e.g. intra-city neighbourhoods) for longer time periods. Also, the outputs by SUEWS can be used as boundary conditions for CFD simulation.

We find that climate, plan area fraction and season combine to impact the NVP. Our findings improve current understanding and design of NVP of urban buildings from a local climate perspective. Local climate in denser areas have been shown to reduce NVP due to warmer outdoor air temperatures on several summer days in Basel (cf. the rural area)

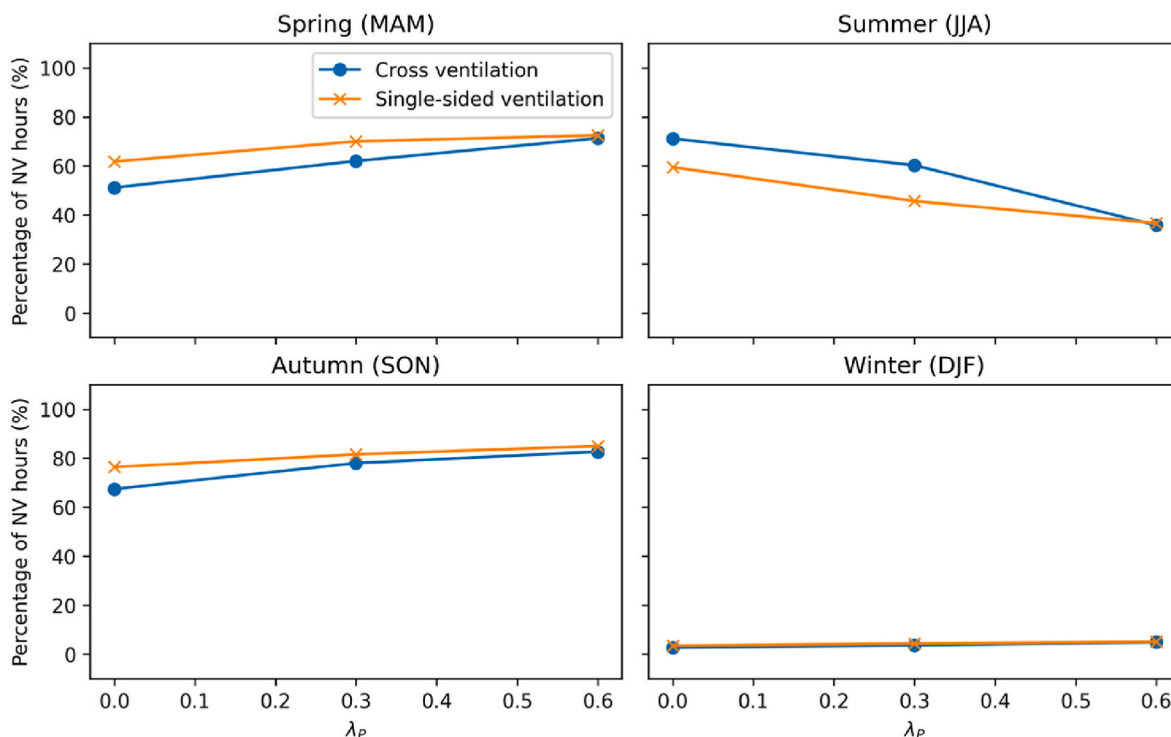


Fig. 15. Shanghai seasonal upper floor for two ventilation modes (percentage of NV hours) for two ventilation modes.

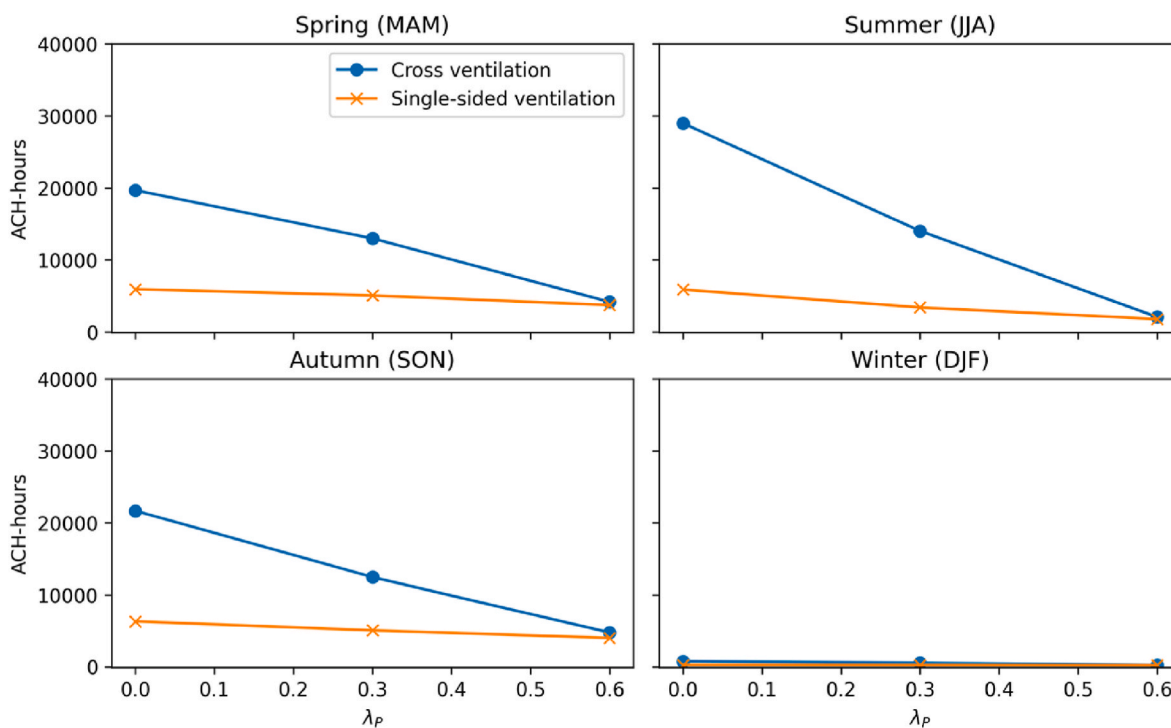


Fig. 16. Seasonal upper floor ACH-hours in Shanghai for two ventilation modes.

[10] and reduced wind speeds from increasing λ_p ($0 \rightarrow 0.2$) reducing annual mean wind-driven ventilation rate by up to 35% [15]. Given these studies, our findings further suggest that under different conditions, increasing the λ_p can either increase or decrease the NVP. For example, in summer, when the λ_p increases from 0 to 0.6, NV-hours increase by around 10% in Harbin (very cold) but decrease by around 43% in Guangzhou (warm winter hot summer). However, a critical

disadvantage of urban areas is the low wind speeds, which leads to lower ventilation rates (e.g. Harbin: annual median ventilation rate reduced by 50% at $\lambda_p = 0.3$ and 85% at $\lambda_p = 0.6$). Hence, we should consider both NV-hours and ACH-hours. It is also found that single-sided ventilation can be as effective as cross ventilation in dense urban areas due to the low wind speed regardless of the metric used.

In this study we consider three metrics: NV-hour, ACH-hour, and

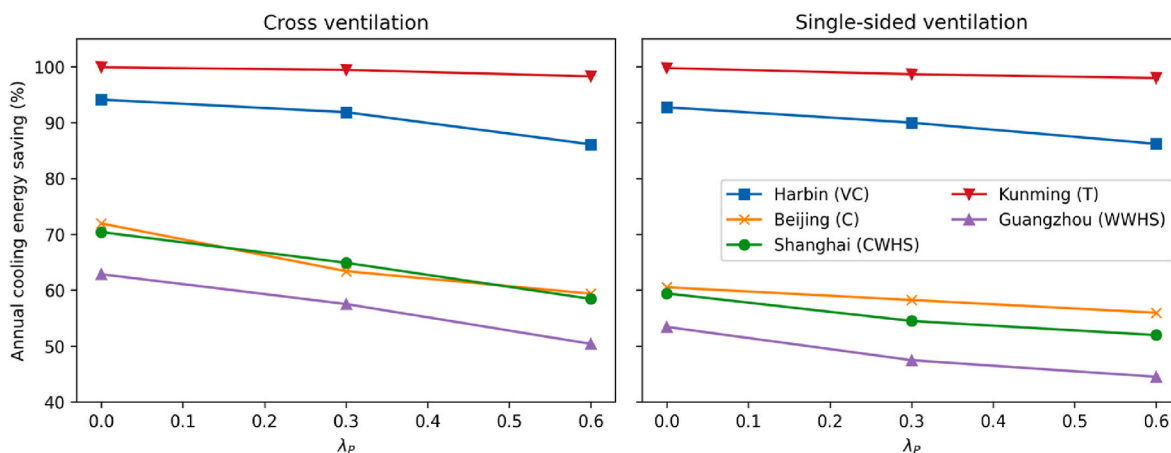


Fig. 17. Seasonal upper floor annual cooling energy saving (Eq. (10), percentages) in five climates (colour) for two ventilation modes.

cooling energy saving. The NV-hour, commonly used to measure NVP, gives the duration (in hours) suitable for natural ventilation. This metric is appropriate when considering general buildings without specific ventilation requirements. Limitation of the NV-hour metric includes its primary reliance on thermal comfort based on indoor temperature and considers only a minimum ventilation rate limit, disregarding variations in ventilation rates determined by wind speed. To address this limitation, we introduce the ACH-hour, which incorporates ventilation rates based on the NV-hour and accounts for the influence of wind speed. The ACH-hour can offset the impact of temperature by considering high wind speeds and larger ventilation rates. For instance, even though Kunming has a milder climate and more NV-hours, the annual ACH-hours in Harbin are greater at $\lambda_p = 0$. Additionally, ACH-hours consistently decrease as λ_p increases. Therefore, the ACH-hour is more appropriate when ventilation rate is a critical factor. Whilst, the cooling energy saving metric (units: %) is influenced by both NVP and the original cooling demand. Climates with cooler summers, such as Harbin and Kunming, have higher percentages of cooling energy saving. This metric is particularly relevant for buildings with mixed-mode ventilation systems. Hence, these metrics are useful for different applications when considering the building and climate being evaluated.

Our approach offers a quick assessment of NVP for buildings in the urban environment. We model idealised neighbourhoods with simplified building models based on relevant observations and standards, although we acknowledge that real cities are more complex. Natural ventilation depends on factors like building and room geometry. In this study we use a simplified shoebox model without interior partitions to maximise cross-ventilation, but real buildings with multiple rooms may have lower cross-ventilation rates, approaching single-sided ventilation. Hence, in more realistic scenarios, NVP for cross-ventilation may resemble that of single-sided ventilation.

Additionally, we assume consistent human activities across regions, overlooking any resulting modifications to anthropogenic heat emissions. Local socioeconomic conditions and population density cause large intra-city emission variability. In our study the neighbourhood density accounted for but not the overall inter-city differences in mean city-wide population density. The latter vary from >2000 people per km^2 in Shanghai to around 900 people per km^2 in Kunming [108]. Higher population densities often correspond to increased anthropogenic heat emissions, resulting in higher urban air temperatures that affect NVP. Densely populated neighbourhoods can have greater anthropogenic heat emissions due to increased building energy consumption and traffic-related emissions. Accounting for these variables can impact NVP results. Detailed data can be used to model anthropogenic heat emissions in different neighbourhoods using SUEWS.

Our findings should be representative of similar climates and neighbourhoods, but future studies could focus on more detailed

information on neighbourhoods in real cities where the variance in NVP might be greater. Existing evaluations suggest that the SUEWS model has acceptable accuracy, although the C_p values should be changed with building geometry. We have only considered buildings and grass in our study and have ignored the impact of trees, which could modify the wind field [79] and radiative fluxes [80] and affect the natural ventilation of nearby buildings. Although trees can be modelled in EnergyPlus (e.g. Ref. [109]), to modify wind pressure coefficients on nearby building facets, measurements or CFD simulations are still necessary. Therefore, our approach can be extended with additional data. Additionally, air and noise pollution, which could be high in dense urban areas, may further reduce NVP (as noted in Table 1), but this is beyond the scope of this study and could be considered in future work.

CRediT authorship contribution statement

Xiaoxiong Xie: Writing – review & editing, Writing – original draft, Visualization, Software, Methodology, Investigation. **Zhiwen Luo:** Writing – review & editing, Supervision, Methodology, Funding acquisition, Conceptualization. **Sue Grimmmond:** Writing – review & editing, Supervision, Methodology, Funding acquisition. **Ting Sun:** Writing – review & editing, Software, Methodology.

Declaration of competing interest

The authors declare that they have no known competing financial interests or personal relationships that could have appeared to influence the work reported in this paper.

Data availability

Data will be made available on request.

Acknowledgements

This work has been funded as part of NERC-COSMA (NE/S005889/1) and ERC urbisphere (855005).

References

- [1] UN, The Paris Agreement, 2015.
- [2] UNEP, Global Status Report for Buildings and Construction: towards a Zero-Emission, Efficient and Resilient Buildings and Construction Sector, 2020. Nairobi, 2020.
- [3] CABEE, China Building Energy Consumption and Carbon Emission Research Report, 2021.

- [4] S.J. Emmerich, W.S. Dols, J.W. Axley, Natural Ventilation Review and Plan for Design and Analysis Tools, National Institute of Standards and Technology, Gaithersburg, 2001.
- [5] Z. Luo, J. Zhao, J. Gao, L. He, Estimating natural-ventilation potential considering both thermal comfort and IAQ issues, *Build. Environ.* 42 (2007) 2289–2298.
- [6] N. Yoon, L. Norford, A. Malkawi, H. Samuelson, M.A. Piette, Dynamic metrics of natural ventilation cooling effectiveness for interactive modeling, *Build. Environ.* 180 (2020), 106994.
- [7] R. Aynsley, Estimating summer wind driven natural ventilation potential for indoor thermal comfort, *J. Wind Eng. Ind. Aerod.* 83 (1999) 515–525.
- [8] L. Yang, G. Zhang, Y. Li, Y. Chen, Investigating potential of natural driving forces for ventilation in four major cities in China, *Build. Environ.* 40 (2005) 738–746.
- [9] C. Ghiaus, F. Allard, M. Santamouris, C. Georgakis, F. Nicol, Urban environment influence on natural ventilation potential, *Build. Environ.* 41 (2006) 395–406.
- [10] M. Germano, Assessing the natural ventilation potential of the Basel region, *Energy Build.* 39 (2007) 1159–1166.
- [11] R. Yao, B. Li, K. Steemers, A. Short, Assessing the natural ventilation cooling potential of office buildings in different climate zones in China, *Renew. Energy* 34 (2009) 2697–2705.
- [12] W. Yin, G. Zhang, W. Yang, X. Wang, Natural ventilation potential model considering solution multiplicity, window opening percentage, air velocity and humidity in China, *Build. Environ.* 45 (2010) 338–344.
- [13] I. Oropeza-Perez, P.A. Østergaard, Potential of natural ventilation in temperate countries—a case study of Denmark, *Appl. Energy* 114 (2014) 520–530.
- [14] G.A. Faggianelli, A. Brun, E. Wurtz, M. Muselli, Natural cross ventilation in buildings on Mediterranean coastal zones, *Energy Build.* 77 (2014) 206–218.
- [15] Y. Li, X. Li, Natural ventilation potential of high-rise residential buildings in northern China using coupling thermal and airflow simulations, *Build. Simulat.* 8 (2015) 51–64.
- [16] K.N. Patil, S.C. Kaushik, Study of climatic potential for natural ventilation in buildings for typical Indian cities, *Int. J. Vent.* 13 (2015) 369–380.
- [17] K. Hiyaama, L. Glicksman, Preliminary Design Method for Naturally Ventilated Buildings Using Target Air Change Rate and Natural Ventilation Potential Maps in the United States, 2015.
- [18] Z. Cheng, L. Li, W.P. Bahnfleth, Natural ventilation potential for gymnasia – case study of ventilation and comfort in a multisport facility in northeastern United States, *Build. Environ.* 108 (2016) 85–98.
- [19] F. Causone, Climatic potential for natural ventilation, *Architect. Sci. Rev.* 59 (2016) 212–228.
- [20] Z. Tong, Y. Chen, A. Malkawi, Z. Liu, R.B. Freeman, Energy saving potential of natural ventilation in China: the impact of ambient air pollution, *Appl. Energy* 179 (2016) 660–668.
- [21] Z. Tong, Y. Chen, A. Malkawi, Estimating natural ventilation potential for high-rise buildings considering boundary layer meteorology, *Appl. Energy* 193 (2017) 276–286.
- [22] N.R. Martins, G. Carrilho Da Graça, Simulation of the Effect of Fine Particle Pollution on the Potential for Natural Ventilation of Non-domestic Buildings in European Cities, 2017.
- [23] Y. Chen, Z. Tong, A. Malkawi, Investigating natural ventilation potentials across the globe: regional and climatic variations, *Build. Environ.* 122 (2017) 386–396.
- [24] Z. Tan, X. Deng, Assessment of natural ventilation potential for residential buildings across different climate zones in Australia, *Atmosphere (Basel)* 8 (2017) 177.
- [25] N. Pestic, J. Roset Calzada, A. Muros Alcojor, Natural ventilation potential of the Mediterranean coastal region of Catalonia, *Energy Build.* 169 (2018) 236–244.
- [26] J. Cheng, D. Qi, A. Katal, L. Wang, T. Stathopoulos, Evaluating Wind-Driven Natural Ventilation Potential for Early Building Design, 2018.
- [27] B. Wang, A. Malkawi, Design-based natural ventilation evaluation in early stage for high performance buildings, *Sustain. Cities Soc.* 45 (2019) 25–37.
- [28] Y. Chen, Z. Tong, W. Wu, H. Samuelson, A. Malkawi, L. Norford, Achieving natural ventilation potential in practice: control schemes and levels of automation, *Appl. Energy* 235 (2019) 1141–1152.
- [29] V. Costanzo, R. Yao, T. Xu, J. Xiong, Q. Zhang, B. Li, Natural ventilation potential for residential buildings in a densely built-up and highly polluted environment. A case study, *Renew. Energy* 138 (2019) 340–353.
- [30] N.R.M. Sakiyama, L. Mazzaferro, J.C. Carlo, T. Bejat, H. Garrecht, Natural ventilation potential from weather analyses and building simulation, *Energy Build.* 231 (2021), 110596.
- [31] U.S. Department of Energy, Chapter 1: overview, in: *EnergyPlus Version 9.4.0 Documentation: Engineering Reference*, 2020, pp. 20–24.
- [32] TRNSYS, TRNSYS 17: Mathematical Reference, 2009.
- [33] D. Yan, J. Xia, W. Tang, F. Song, X. Zhang, Y. Jiang, DeST — an integrated building simulation toolkit Part I: fundamentals, *Build. Simulat.* 12 (1) (2008) 95–110, 2008.
- [34] Integrated Environmental Solutions, MacroFlo calculation methods [WWW Document]. <https://help.iesve.com/ve2018/>, 2018.
- [35] A.S. Andelković, I. Mujan, S. Dakić, Experimental validation of a EnergyPlus model: application of a multi-storey naturally ventilated double skin façade, *Energy Build.* 118 (2016) 27–36.
- [36] N. Fumo, P. Mago, R. Luck, Methodology to estimate building energy consumption using EnergyPlus Benchmark Models, *Energy Build.* 42 (2010) 2331–2337.
- [37] K.P. Lam, J. Zhao, E.B. Ydstie, J. Wirrick, M. Qi, J. Park, An EnergyPlus whole building energy model calibration method for office buildings using occupant behavior data mining and empirical data, in: 2014 ASHRAE/IBPSA-USA Building Simulation Conference, 2014, pp. 160–167.
- [38] M. Royapoor, T. Roskilly, Building model calibration using energy and environmental data, *Energy Build.* 94 (2015) 109–120.
- [39] E.M. Ryan, T.F. Sanquist, Validation of building energy modeling tools under idealized and realistic conditions, *Energy Build.* 47 (2012) 375–382.
- [40] J.L.M. Hensen, Jan, Simulation of building energy and indoor environmental quality - some weather data Issues, *Int. Work. Clim. data their Appl. Eng.* (1999) 1–15.
- [41] T.R. Oke, G. Mills, A. Christen, J.A. Voogt, *Urban Climates*, Cambridge University Press, Cambridge, 2017.
- [42] T. van Hooff, B. Blocken, On the effect of wind direction and urban surroundings on natural ventilation of a large semi-enclosed stadium, *Comput. Fluids* 39 (2010) 1146–1155.
- [43] W. Yang, Y. Quan, X. Jin, Y. Tamura, M. Gu, Influences of equilibrium atmosphere boundary layer and turbulence parameter on wind loads of low-rise buildings, *J. Wind Eng. Ind. Aerod.* 96 (2008) 2080–2092.
- [44] A. Zhang, C. Gao, L. Zhang, Numerical simulation of the wind field around different building arrangements, *J. Wind Eng. Ind. Aerod.* 93 (2005) 891–904.
- [45] WMO, Guidance to Measuring, Modelling and Monitoring the Canopy Layer Urban Heat Island, vol. 2021, EMS Annual Meeting, Geneva, 2023.
- [46] C.S.B. Grimmond, T.R. Oke, D.G. Steyn, Urban water balance: 1. A model for daily totals, *Water Resour. Res.* 22 (1986) 1397–1403.
- [47] C.S.B. Grimmond, T.R. Oke, Heat storage in urban areas: local-scale observations and evaluation of a simple model, *J. Appl. Meteorol.* 38 (1999) 922–940.
- [48] L. Allen, F. Lindberg, C.S.B. Grimmond, Global to city scale urban anthropogenic heat flux: model and variability, *Int. J. Climatol.* 31 (2011) 1990–2005.
- [49] D.J. Sailor, A review of methods for estimating anthropogenic heat and moisture emissions in the urban environment, *Int. J. Climatol.* 31 (2011) 189–199.
- [50] X. Xie, Z. Luo, S. Grimmond, T. Sun, W. Morrison, Impact of inter-building longwave radiative exchanges on building energy performance and indoor overheating, *Build. Environ.* 209 (2022), 108628.
- [51] A. Boccalatte, M. Fossa, L. Gaillard, C. Menezo, Microclimate and urban morphology effects on building energy demand in different European cities, *Energy Build.* 224 (2020), 110129.
- [52] A. Kamal, S.M.H. Abidi, A. Mahfouz, S. Kadam, A. Rahman, I.G. Hassan, L. Wang, Impact of urban morphology on urban microclimate and building energy loads, *Energy Build.* 253 (2021), 111499.
- [53] Y. Liu, R. Stouffs, A. Tablada, N.H. Wong, J. Zhang, Comparing micro-scale weather data to building energy consumption in Singapore, *Energy Build.* 152 (2017) 776–791.
- [54] S. Magli, C. Lodi, L. Lombroso, A. Muscio, S. Teggi, Analysis of the urban heat island effects on building energy consumption, *Int. J. Energy Environ. Eng.* 6 (2015) 91–99.
- [55] X. Xie, Z. Luo, S. Grimmond, L. Blunn, Use of wind pressure coefficients to simulate natural ventilation and building energy for isolated and surrounded buildings, *Build. Environ.* 230 (2023), 109951.
- [56] Y. Toparlar, B. Blocken, B. Maiheu, G.J.F. van Heijst, A review on the CFD analysis of urban microclimate, *Renew. Sustain. Energy Rev.* 80 (2017) 1613–1640.
- [57] R. Ramponi, I. Gaetani, A. Angelotti, Influence of the urban environment on the effectiveness of natural night-ventilation of an office building, *Energy Build.* 78 (2014) 25–34.
- [58] C.S.B. Grimmond, T.R. Oke, Aerodynamic properties of urban areas derived from analysis of surface form, *J. Appl. Meteorol.* 38 (1999) 1262–1292.
- [59] N.E. Theeuwes, R.J. Ronda, I.N. Harman, A. Christen, C.S.B. Grimmond, Parametrizing horizontally-averaged wind and temperature profiles in the urban roughness sublayer, *Boundary-Layer Meteorol.* 173 (2019) 321–348.
- [60] L. Järvi, C.S.B. Grimmond, A. Christen, The surface urban energy and water balance scheme (SUEWS): evaluation in Los Angeles and Vancouver, *J. Hydrol.* 411 (2011) 219–237.
- [61] H.C. Ward, S. Kotthaus, L. Järvi, C.S.B. Grimmond, Surface urban energy and water balance scheme (SUEWS): development and evaluation at two UK sites, *Urban Clim.* 18 (2016) 1–32.
- [62] C.S.B. Grimmond, M. Blackett, M.J. Best, J.-J. Baik, S.E. Belcher, J. Beringer, S. I. Bohnenstengel, I. Calmet, F. Chen, A. Coutts, A. Dandou, K. Fortuniak, M. L. Gouvea, R. Hamdi, M. Hendry, M. Kanda, T. Kawai, Y. Kawamoto, H. Kondo, E.S. Krayenhoff, S.-H. Lee, T. Loridan, A. Martilli, V. Masson, S. Miao, K. Oleson, R. Ooka, G. Pigeon, A. Porson, Y.-H. Ryu, F. Salamanca, G.J. Steeneveld, M. Tombrou, J.A. Voogt, D.T. Young, N. Zhang, Initial results from phase 2 of the international urban energy balance model comparison, *Int. J. Climatol.* 31 (2011) 244–272.
- [63] C.S.B. Grimmond, M. Blackett, M.J. Best, J. Barlow, J.J. Baik, S.E. Belcher, S. I. Bohnenstengel, I. Calmet, F. Chen, A. Dandou, K. Fortuniak, M.L. Gouvea, R. Hamdi, M. Hendry, T. Kawai, Y. Kawamoto, H. Kondo, E.S. Krayenhoff, S. H. Lee, T. Loridan, A. Martilli, V. Masson, S. Miao, K. Oleson, G. Pigeon, A. Porson, Y.H. Ryu, F. Salamanca, L. Shashua-Bar, G.J. Steeneveld, M. Tombrou, J. Voogt, D. Young, N. Zhang, The international urban energy balance models comparison project: first results from phase 1, *J. Appl. Meteorol. Climatol.* 49 (2010) 1268–1292.
- [64] F. Lindberg, C.S.B. Grimmond, A. Gabey, B. Huang, C.W. Kent, T. Sun, N. E. Theeuwes, L. Järvi, H.C. Ward, I. Capel-Timms, Y. Chang, P. Jonsson, N. Krave, D. Liu, D. Meyer, K.F.G. Olofson, J. Tan, D. Wästberg, L. Xue, Z. Zhang, Urban Multi-scale Environmental Predictor (UMEP): an integrated tool for city-based climate services, *Environ. Model. Software* 99 (2018) 70–87.
- [65] T. Sun, S. Grimmond, A Python-enhanced urban land surface model SuPy (SUEWS in Python, v2019.2): development, deployment and demonstration, *Geosci. Model Dev.* 12 (2019) 2781–2795.

- [66] Y. Tang, T. Sun, Z. Luo, H. Omidvar, N. Theeuwes, X. Xie, J. Xiong, R. Yao, S. Grimmond, Urban meteorological forcing data for building energy simulations, *Build. Environ.* 204 (2021), 108088.
- [67] M.E. Fernández, N. Picone, J.O. Gentili, A.M. Campo, Analysis of the urban energy balance in Bahía Blanca (Argentina), *Urban Clim.* 37 (2021), 100856.
- [68] F. Lindberg, K.F.G. Olofson, T. Sun, C.S.B. Grimmond, C. Feigenwinter, Urban storage heat flux variability explored using satellite, meteorological and geodata, *Theor. Appl. Climatol.* 141 (2020) 271–284.
- [69] S. Rafael, H. Martins, M.J. Matos, M. Cerqueira, C. Pio, M. Lopes, C. Borrego, Application of SUEWS model forced with WRF: energy fluxes validation in urban and suburban Portuguese areas, *Urban Clim.* 33 (2020), 100662.
- [70] M. Havu, L. Kulmala, P. Kolari, T. Vesala, A. Riikonen, L. Järvi, Carbon sequestration potential of street tree plantings in Helsinki, *Biogeosciences* 19 (2022) 2121–2143.
- [71] R. Wiegels, F. Chapa, J. Hack, High resolution modeling of the impact of urbanization and climate on energy partitioning on the water and energy balance, *Urban Clim.* 39 (2021), 100961.
- [72] B. Augusto, P. Roebeling, S. Rafael, J. Ferreira, A. Ascenso, C. Bodilis, Short and medium- to long-term impacts of nature-based solutions on urban heat, *Sustain. Cities Soc.* 57 (2020), 102122.
- [73] H.C. Ward, C.S.B. Grimmond, Assessing the impact of changes in surface cover, human behaviour and climate on energy partitioning across Greater London, *Landsc. Urban Plann.* 165 (2017) 142–161.
- [74] M.H. Johnson, Z.J. Zhai, M. Krarti, Performance Evaluation of Network Airflow Models for Natural Ventilation, HVAC and R Research, 2012.
- [75] Z. (John) Zhai, M.H. Johnson, M. El Mankibi, N. Stathopoulos, Review of natural ventilation models, *Int. J. Vent.* 15 (2016) 186–204.
- [76] T. van Hooff, B. Blocken, Y. Tominaga, On the accuracy of CFD simulations of cross-ventilation flows for a generic isolated building: comparison of RANS, LES and experiments, *Build. Environ.* 114 (2017) 148–165.
- [77] I.N. Harman, J.J. Finnigan, A simple unified theory for flow in the canopy and roughness sublayer, *Boundary-Layer Meteorol.* 123 (2007) 339–363.
- [78] T. Sun, L. Järvi, H. Omidvar, N. Theeuwes, F. Lindberg, Z. Li, S. Grimmond, Urban-Meteorology-Reading/SUEWS: 2020a Release, 2020.
- [79] C.W. Kent, K. Lee, H.C. Ward, J.-W. Hong, J. Hong, D. Gatey, S. Grimmond, Aerodynamic roughness variation with vegetation: analysis in a suburban neighbourhood and a city park, *Urban Ecosyst.* 21 (2018) 227–243.
- [80] W. Morrison, S. Kothaus, C.S.B. Grimmond, A. Inagaki, T. Yin, J.P. Gastellu-Etchegorry, M. Kanda, C.J. Merchant, A novel method to obtain three-dimensional urban surface temperature from ground-based thermography, *Remote Sens. Environ.* 215 (2018) 268–283.
- [81] MoHURD, Design Standard for Energy Efficiency of Public Buildings (GB50189-2015), Ministry of Housing and Urban-rural Development, P.R. China, Beijing, 2015.
- [82] H. Hersbach, B. Bell, P. Berrisford, S. Hirahara, A. Horányi, J. Muñoz-Sabater, J. Nicolas, C. Peubey, R. Radu, D. Schepers, A. Simmons, C. Soci, S. Abdalla, X. Abellan, G. Balsamo, P. Bechtold, G. Biavati, J. Bidlot, M. Bonavita, G. De Chiara, P. Dahlgren, D. Dee, M. Diamantakis, R. Dragani, J. Flemming, R. Forbes, M. Fuentes, A. Geer, L. Haimberger, S. Healy, R.J. Hogan, E. Hólm, M. Janisková, S. Keeley, P. Laloyaux, P. Lopez, C. Lupu, G. Radnoti, P. de Rosnay, I. Rozum, F. Vamborg, S. Villaume, J.N. Thépaut, J. Muñoz-Sabater, J. Nicolas, C. Peubey, R. Radu, D. Schepers, A. Simmons, C. Soci, S. Abdalla, X. Abellan, G. Balsamo, P. Bechtold, G. Biavati, J. Bidlot, M. Bonavita, G. Chiara, P. Dahlgren, D. Dee, M. Diamantakis, R. Dragani, J. Flemming, R. Forbes, M. Fuentes, A. Geer, L. Haimberger, S. Healy, R.J. Hogan, E. Hólm, M. Janisková, S. Keeley, P. Laloyaux, P. Lopez, C. Lupu, G. Radnoti, P. Rosnay, I. Rozum, F. Vamborg, S. Villaume, J.N. Thépaut, The ERA5 global reanalysis, *Q. J. R. Meteorol. Soc.* 146 (2020) 1999–2049.
- [83] K. Xu, R. Lu, J. Mao, R. Chen, X.U. Ke, L.U. Riyu, M. Jiangyu, C. Ruidan, Circulation anomalies in the mid-high latitudes responsible for the extremely hot summer of 2018 over northeast Asia, *New Pub KeAi* 12 (2019) 231–237.
- [84] T.R. Oke, G. Mills, A. Christen, J.A. Voogt, *Urban Climates*, Cambridge University Press, Cambridge, 2017.
- [85] J. Liu, Y. Li, C. Zhang, Z. Liu, The effect of high altitude environment on diesel engine performance: comparison of engine operations in Hangzhou, Kunming and Lhasa cities, *Chemosphere* 309 (2022), 136621.
- [86] I.N. Harman, J.J. Finnigan, Scalar concentration profiles in the canopy and roughness sublayer, *Boundary-Layer Meteorol.* 129 (2008) 323–351.
- [87] ANSI/ASHRAE, Standard Method of Test for the Evaluation of Building Energy Analysis Computer Programs, 2011. Atlanta.
- [88] J. Xiong, R. Yao, S. Grimmond, Q. Zhang, B. Li, A hierarchical climatic zoning method for energy efficient building design applied in the region with diverse climate characteristics, *Energy Build.* 186 (2019) 355–367.
- [89] MoHURD, Code for Thermal Design of Civil Building (GB50176-2016), Ministry of Housing and Urban-rural Development, P.R. China, Beijing, 2016.
- [90] U.S. Department of Energy, Chapter 13: alternative modeling processes, in: *EnergyPlus Version 9.4.0 Documentation: Engineering Reference*, 2020, pp. 601–705.
- [91] H.B. Awbi, *Ventilation of Buildings*, Second., Taylor & Francis Group, New York, 2003.
- [92] M. Grosso, Wind pressure distribution around buildings: a parametrical model, *Energy Build.* 18 (1992) 101–131.
- [93] TPU, Aerodynamic Database for Low-Rise Buildings, 2007. Tokyo, Japan.
- [94] H.Y. Zhong, Y. Sun, J. Shang, F.P. Qian, F.Y. Zhao, H. Kikumoto, C. Jimenez-Bescos, X. Liu, Single-sided natural ventilation in buildings: a critical literature review, *Build. Environ.* 212 (2022).
- [95] P.R. Warren, Ventilation through openings on one wall only, in: *International Conference on Heat and Mass Transfer in Buildings*, Dubrovnik, 1977.
- [96] P.R. Warren, L.M. Parkins, Single-sided ventilation through open windows, in: *Document - Swedish Council for Building Research*, 1984, p. 487.
- [97] H.L. Gough, J.F. Barlow, Z. Luo, M.F. King, C.H. Haliotis, C.S.B. Grimmond, Evaluating single-sided natural ventilation models against full-scale idealised measurements: impact of wind direction and turbulence, *Build. Environ.* 170 (2020), 106556.
- [98] T. Yamanaka, H. Kotani, K. Iwamoto, M. Kato, Natural, wind-forced ventilation caused by turbulence in a room with a single opening, *Int. J. Vent.* (2006).
- [99] U.S. Department of Energy, Chapter 8: air heat balance manager/processes, in: *EnergyPlus Version 9.4.0 Documentation: Engineering Reference*, 2020, pp. 58–168.
- [100] ANSI/ASHRAE, *Ventilation for Acceptable Indoor Air Quality*, 2013.
- [101] MoHURD, Evaluation Standard for Indoor Thermal Environment in Civil Buildings (GB/T50785-2012), Ministry of Housing and Urban-rural Development, P.R. China, Beijing, 2012.
- [102] F. Nicol, M. Humphreys, Derivation of the adaptive equations for thermal comfort in free-running buildings in European standard EN15251, *Build. Environ.* 45 (2010) 11–17.
- [103] J. Sundell, H. Levin, W.W. Nazaroff, W.S. Cain, W.J. Fisk, D.T. Grimsrud, F. Gyntelberg, Y. Li, A.K. Persily, A.C. Pickering, J.M. Samet, J.D. Spengler, S. T. Taylor, C.J. Weschler, Ventilation rates and health: multidisciplinary review of the scientific literature, *Indoor Air* 21 (2011) 191–204.
- [104] S.J. Mei, J.T. Hu, D. Liu, F.Y. Zhao, Y. Li, Y. Wang, H.Q. Wang, Wind driven natural ventilation in the idealized building block arrays with multiple urban morphologies and unique package building density, *Energy Build.* 155 (2017) 324–338.
- [105] ASHRAE, *ASHRAE Handbook : Fundamentals*, American Society of Heating, Refrigerating and Air-Conditioning Engineers, Atlanta, 2005.
- [106] U.S. Department of Energy, Chapter 5: climate, sky and solar/shading calculations, in: *EnergyPlus Version 9.4.0 Documentation: Engineering Reference*, 2020, pp. 187–224.
- [107] X. Yang, L. Zhao, M. Bruse, Q. Meng, An integrated simulation method for building energy performance assessment in urban environments, *Energy Build.* 54 (2012) 243–251.
- [108] G. Xu, L. Jiao, M. Yuan, T. Dong, B. Zhang, C. Du, How does urban population density decline over time? An exponential model for Chinese cities with international comparisons, *Landsc. Urban Plann.* 183 (2019) 59–67.
- [109] C.-M. Hsieh, J.-J. Li, L. Zhang, B. Schweger, Effects of tree shading and transpiration on building cooling energy use, *Energy Build.* 159 (2018) 382–397.